学 位 論 文

Ground-state properties of electron systems in the strong-correlation limit

強相関極限での電子系の基底状態の性質

平成９年12月 博士(理学)申請

東京大学大学院理学系研究科
物理学専攻

河 野 昌 仙

論文の内容の要旨

論文題目　Ground-state properties of electron systems in the strong-correlation limit

日本語題名　強相関極限での電子系の基底状態の性質

氏名　河野　昌仙

電子相関によって引き起こされる現象には様々なものがあるが、近年特に、低次元強相関電子系の低温での性質に注目が集まっている。その理由として、高温超伝導体を始めとする擬２次元系や擬１次元系と見なせる物質が、実験的に合成されるようになったことや、数値計算により、低次元系について多くの情報が得られるようになったことなどの技術的側面が挙げられる。また、量子多体効果が顕著に現われるので、従来の平均場的解析で理解されない新しい現象が見いだせる可能性があることも注目を集めている理由の１つであると考えられる。この論文では、電子相関の強い極限を考えることによって、低次元強相関電子系のいくつかの基本的な側面を明らかにすることを目的とする。議論を単純化するために、この論文では、バイパータイトのハバード型の模型の基底状態に話を限ることにする。

この論文は大きく分けて２つの部分から成る。第１部では、斥力ハバード模型を、第２部では、近接サイト間斥力を含む引力ハバード模型を考える。第１部の始めでは、１次元電子系の特徴であるスピンと電荷の分離を実感するために、$U \to +\infty$ ハバード鎖についてのベーテ仮設法の結果をレビューする。続いて、ハバード鎖の特殊性を部分的に排除した模型として梯子ハバード模型を考える。特に、$U = +\infty$ での強磁性と 1/4 フィリングでの金属ー絶縁体転移に注目し、ハバード鎖の性質との類似点と相違点について考察する。また、２次元強相関電子系との関連をみるために、２次元 t-J 模型の基底状態について、現在までに報告されている事柄を簡単にまとめる。第２部では、超伝導ー絶縁体転移を議論するために、近接サイト間斥力を含む引力ハバード模型を考える。引力が大きな極限では、有効模型としてイジング異方性をもつスピン$\frac{1}{2}XXZ$模型が得られるので、拡張 $U \to -\infty$ ハバード模型の超伝導ー絶縁体転移を調べるために、それと等価なスピン$\frac{1}{2}XXZ$模型の磁化過程を調べる。始めに、１次元スピン$\frac{1}{2}XXZ$模型の磁化過程についてのベーテ仮設法の結果を簡単に紹介する。続いて、２次元、３次元でのスピン$\frac{1}{2}XXZ$模型の磁化過程について数値的に調べた結果を報告する。以下、この論文の中心部分である、$U = +\infty$ 梯子ハバード模型の基底状態と、２次元、３次元のスピン$\frac{1}{2}XXZ$模型の磁化過程について述べる。

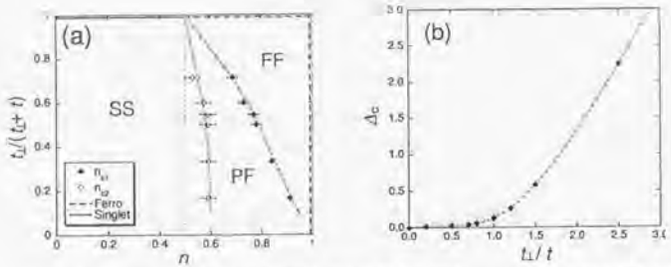

図 1: (a)$U=+\infty$ 梯子ハバード模型の基底状態の磁化に関する相図。$n=1$ は、長岡の定理より、完全強磁性状態。$t_\perp/t\to\infty$ で、$n\le 0.5$ では、スピン一重項、$n>0.5$ では、完全強磁性状態が基底状態。SS、FF、PF は、それぞれ、スピン一重項、完全強磁性状態、不完全強磁性状態の領域を表す。n は電子濃度で、$n=1$ がハーフフィリングである。(b)$U=+\infty$ 梯子ハバード模型の 1/4 フィリングでの電荷ギャップΔ_c。

(I) $U=+\infty$ 梯子ハバード模型における強磁性。
1 次元ハバード模型では、Lieb-Mattis の定理により、強磁性状態は実現しないことが知られているが、梯子ハバード模型では、強磁性状態が有限のホール濃度で実現し得ることを解析的、数値的手法を用いて示すことができた。まず、$U=+\infty$ 梯子ハバード模型について、鎖間ホッピング $t_\perp$ が鎖内ホッピング t に比べて大きな極限 ($t_\perp/t\to\infty$) を調べる。電子密度 $n\le 0.5$(1/4 フィリング以下) では、梯子模型の $t^2/t_\perp$ のオーダーまでの有効模型が、$U\to+\infty$ ハバード鎖の t^2/U までのオーダーの有効模型と一致することが示せるので、$t_\perp/t$ が大きな極限では、偶数電子系で基底状態がスピン一重項になることが分かった。一方、電子密度 $n>0.5$ に関しては、Perron-Frobenius の定理を用い、t に関して 1 次オーダーのまでの有効模型が強磁性基底状態をもつことを厳密に示すことができた。以上より、$t_\perp/t$ が大きな極限での $U=+\infty$ 梯子ハバード模型の基底状態が、$n\le 0.5$ では、スピン一重項になり、$n>0.5$ では、強磁性状態になることが分かった。有限の $t_\perp/t$ の基底状態については、密度行列繰り込み群 (DMRG) 法という数値計算方法を用いて調べた。その結果、図 1 (a) に示すように、有限の $t_\perp/t$ でも、強磁性状態が基底状態になり得ることが分かった。また、$t_\perp/t$ が大きな方が、強磁性状態が安定であることも、この図から推測される。さらに、梯子 t-J 模型についても同様な計算をしたところ、反強磁性的相互作用 J を導入しても、不完全強磁性状態が有限の領域で存在することも、DMRG 法の精度の範囲内で確かめることができた。

(II) $U=+\infty$ 梯子ハバード模型の 1/4 フィリングでの金属ー絶縁体転移。
$U=+\infty$ 梯子ハバード模型の 1/4 フィリングについて、$t_\perp$ が大きな極限では、$2t_\perp$ の大きさの電荷ギャップが開くが、この電荷ギャップは、$t_\perp$ を小さくしたときに、どのように振る舞うのだろうか。また、電荷ギャップがなくなる $t_\perp$ の大きさはどのくらいなのだろうか。これらの点を明らかにするために、DMRG 法を用いて調べたところ、図 1 (b) に示すような結果が得られた。この図から、弱相関の場合にギャップレスであった領域 ($t_\perp/t\le 1$) でも、電荷ギャップが開いていることが分かる。次に、ギャップがなくなる $t_\perp/t$

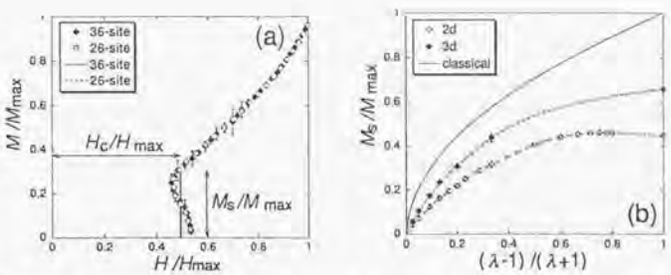

図 2: (a) 2 次元スピン$\frac{1}{2}XXZ$模型の磁化曲線。異方性パラメータ$\lambda=2$。$H_{\max}$ と $M_{\max}$ は、それぞれ、飽和磁場と磁化の最大値を表す。縦線は、XY 相とネール相との共存線を表す。(b) 2 次元、3 次元のスピン$\frac{1}{2}XXZ$模型の磁化の跳び M_s。イジング模型の場合は、$M_s/M_{\max}=1$ である。

を求めるために、基底状態のスペクトラルフローの振る舞いを調べた。その結果、$t_\perp/t=0.001$ で既に絶縁体であることを数値的に示すことができた。$U=+\infty$ という特殊性を考慮すると、$t_\perp/t\neq 0$ では、任意の $t_\perp/t$ で絶縁体であることが推測される。ここで、これら $U=+\infty$ の性質を U が小さい場合と比較する。U が小さいときには、有効的に結合バンドと反結合バンドで記述されるので、$t_\perp/t>1$ の 1/4 フィリングでは、1 次元ハバード模型と同じ金属ー絶縁体転移が起こり、電荷ギャップの大きさは、U が小さいところでは、指数関数的に小さいことが知られている。一方、$U=+\infty$ で $t_\perp$ が大きなときも、1 次元ハバード模型との対応がつくので、この場合にも同様な金属ー絶縁体転移が起こることが期待される。しかし、上で調べたように、$U=+\infty$ 梯子ハバード模型では、鎖間ホッピング $t_\perp$ を相互作用 U と見なすような 1 次元ハバード模型に対応しているので、金属ー絶縁体転移を引き起こす主な原因は、弱相関領域と強相関領域では、異なっていると思われる。つまり、弱相関領域では、結合バンド内での U による金属ー絶縁体転移とみなせるのに対し、強相関領域では、バンド間の $t_\perp$ による金属ー絶縁体転移とみなすことができると考えられる。

(III) イジング異方性をもつスピン$\frac{1}{2}XXZ$模型の磁化過程。
1 次元の場合には、磁場 H に対して磁化 M が $M\propto\sqrt{H-H_c}$ のように振る舞い、2 次の相転移であることが知られている。これに対し、無限次元で正当化されるような古典スピン系の場合には、スピンフロップと呼ばれる 1 次相転移を起こすことが知られている。それでは、2 次元、3 次元ではどのような相転移が起きるのだろうか。そこで、この論文では、2 次元、3 次元のイジング異方性をもつスピン$\frac{1}{2}XXZ$模型の磁化過程について、数値的に調べた結果を報告する。数値計算方法は、クラスターアルゴリズムという量子モンテカルロ法と厳密対角化法を用いた。数値計算の結果、図 2 (a) に示すような磁化曲線が得られた。この図から明らかなように、2 次元のイジング異方性をもつスピン$\frac{1}{2}XXZ$模型は、1 次相転移を起こすことが分かった。さらに、この 1 次転移における磁化の跳び M_s の異方性パラメータλ依存性を調べたところ、図 2 (b) に示すような結果が得られた。異方性パラメータλは、$\lambda=1$ が SU(2) ハイゼンベルグ模型、$\lambda\to\infty$ がイジング異方性が大きな極限に対応している。この図から、$\lambda>1$ では 1 次相転移を起こすこと

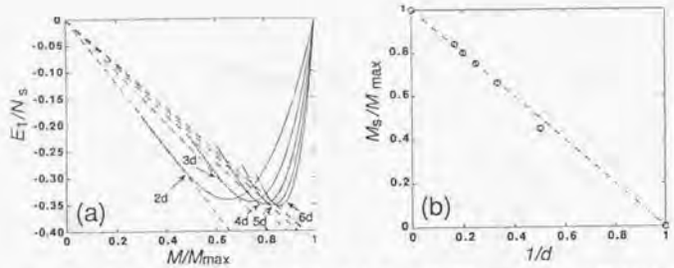

図 3: (a) イジング極限 ($\lambda \to \infty$) での 1 次の摂動エネルギー。直線は、マクスウェル構築によって決めた XY 相とネール相との共存線を表す。(b) イジング極限での磁化の跳び M_s。d は空間次元を表す。

が分かり、また、イジング極限とイジング模型の場合とでは、磁化の跳びの大きさが有意に異なっているということも分かった。このことは、$\lambda \to \infty$ での摂動を考えると理解できる。つまり、2 次元以上の場合は、磁化が大きなところでは、λ^0 のオーダーの摂動が存在するが、磁化がゼロ付近では、λ^{-1} のオーダーが最低次の摂動になっているからである。このことは、量子揺らぎがあるときには、イジング極限での磁化の跳びが、イジング模型の場合よりも小さくなることを意味している。実際、数値的に $\lambda \to \infty$ での磁化の跳び $M_s(\lambda \to \infty)$ を評価すると、図 3 のようになる。1 次元では、2 次相転移であるため、$M_s(\lambda \to \infty) = 0$ であるが、2 次元、3 次元、…と次元を上げていくと、$M_s(\lambda \to \infty)$ は次第に増大し、無限次元でイジング模型のもの ($M_s = M_{\rm max}$) と一致することが分かる。以上のことから、対応する拡張引力ハバード模型 ($U \to -\infty$) について、有限次元では、近接サイト間斥力がどんなに大きくても、均一な超伝導状態が、有限の低電子密度領域で存在することが分かった。また、2 次元、3 次元では、この模型のハーフフィリングでの超伝導－絶縁体転移は 1 次転移であることも分かった。

論文の主な結果は 以下のものである。(i) バイパータイトのハバード模型の有限ホール濃度で、強磁性基底状態が実現し得ることを、解析的、数値的手法を用いて例証した。(ii)$U = \infty$ 梯子ハバード模型の 1/4 フィリングでの基底状態は、$|t_\perp/t| \geq 0.001$ のときに絶縁体であることを数値的に示すことができた。(おそらく、$t_\perp/t = 0$ を除くすべての $t_\perp/t$ で絶縁体であると推測される。) (iii) イジング異方性をもつスピン $\frac{1}{2}XXZ$ 模型の磁化過程は、2 次元、3 次元では 1 次転移であることを数値的に確かめることができた。(iv) 有限次元では、イジング異方性が大きな極限での磁化の跳びは、イジング模型のものとは有限の大きさの違いがあることが分かった。

以上、強相関電子系の基本的な現象として、遍歴強磁性、金属－絶縁体転移、超伝導－絶縁体転移を取り上げて考察した。それぞれの問題について、強相関極限での簡単化した模型を扱ってきたが、その結果は、様々な強相関系に共通するいくつかの側面を表していると考えている。なぜならば、$U = \infty$ ハバード模型やスピン $\frac{1}{2}XXZ$ 模型は、様々な模型の強相関極限とみなすことができるからである。例えば、$U = \infty$ ハバード模型は、近藤カップリング J_K が大きな極限での近藤格子模型とみなすこともでき、また、スピン $\frac{1}{2}XXZ$ 模型は、拡張ボゾンハバード模型のオンサイト斥力の大きな極限ともみなすことができる。

Thesis

Ground-state properties of electron systems in the strong-correlation limit

Masanori Kohno

Institute for Solid State Physics,

University of Tokyo

December 1997

Acknowledgements

I would like to express my sincerest gratitude to Professor Minoru Takahashi for continual support, fruitful suggestions and helpful comments. I would also like to thank Dr. K . Kusakabe for his invitation to the area of ferromagnetism and advice on computer programming of exact diagonalization. I am grateful to Dr. F.F. Assaad for stimulating discussions on the Mott transition and suggestions for Monte Carlo simulations. I am also grateful to Prof. F.V. Kusmartsev for his continual encouragement and cordial support. I would also like to express my gratitude to Prof. M. Imada, Prof. M. Ogata, and Prof. H. Tasaki for their helpful comments and discussions. I thank Dr. T. Kawarabayashi, Dr. D. Lidsky, and Dr. E. Williams for their critical reading of manuscripts. I also thank Dr. M. Yajima for computer programming of the density-matrix renormalization method, and Dr. Y. Iino and Dr. M. Troyer for programming of the cluster algorithm. I am also grateful for Mr. K. Kawano, Mr. M. Tsukano and Mr. K. Itoh for stimulating discussions and many fruitful suggestions. I wish to thank the members of the research groups on the third floor in Institute for Solid State Physics.

Part of numerical calculations were performed on the Fujitsu VPP500 and on the Intel Japan PARAGON at Institute for Solid State Physics. The exact diagonalization program is partly based on the subroutine package "TITPACK Ver.2" coded by Prof. H. Nishimori and partly on the subroutines coded by Dr. K. Kusakabe. This research was supported in part by Grants-in-Aid for Scientific Research Fund from the Ministry of Education, Science and Culture.

Finally, I would like to thank my parents and all of my old friends for their continual encouragement and support.

Contents

Chapter 1

General introduction

1.1 Introduction

In materials, competition between Coulomb repulsion and hopping of electrons causes a large variety of phenomena. Some properties of metals are successfully explained by weak-coupling theories such as Landau's Fermi liquid theory[1] and perturbative calculations with respect to the interaction strength. However, there are a lot of phenomena which are difficult to understand from the weak-coupling view-point. For a long time, such phenomena have attracted interest. This is not only due to the possibility of its technological applications, but also due to the difficulty of fundamental understanding of these phenomena. The difficulty mainly comes from its quantum many-body effects and statistical mechanical aspects. Recent interests have been focused on low-temperature properties of low-dimensional systems in the strong-coupling regime. In this situation, quantum fluctuations dominate and require other approaches than the conventional ones such as Hartree-Fock mean-field approximations. Here, let us see some phenomena which are originated from strong electronic correlations.

The Mott transition is a typical phenomenon caused by electronic correlations. Mott pointed out that, if the Coulomb repulsion is strong enough, systems can be insulating, even though they contain an incomplete Brillouin zone[2]. Later, Hubbard demonstrated, by a kind of coherent potential approximation (CPA), that a charge gap opens

at half-filling in the repulsive Hubbard model[3]. Owing to the charge gap, the low-energy physics is effectively described by the antiferromagnetic Heisenberg model, which is derived from the Hubbard model at half-filling in the limit $U \to +\infty$. This antiferromagnetic exchange interaction between localized spins is called as kinetic exchange[4]. Anderson argued the possibility that high-T_c superconductivity[5] is also due to strong electronic correlations[6]. One of the reasons is that low-energy properties of mother compounds of high-T_c superconductors are described by the antiferromagnetic Heisenberg model originated from the kinetic exchange processes.[1]

Another example of unexpected phenomena which are due to strong electronic correlations is Nagaoka's ferromagnetism[7, 8, 9]. Nagaoka's theorem states that, except for one dimension, the ground state of the $U = +\infty$ Hubbard model is ferromagnetic if the number of holes is one. This theorem demonstrates that the ground state of strongly correlated electron systems can be ferromagnetic. Natural questions arising here are whether this ferromagnetic state is stable for finite hole-density, and whether ferromagnetism in real materials is originated from purely electronic correlations. There have been a lot of attempts to answer these questions by investigating itinerant ferromagnetism in Hubbard-type models. However, few results are obtained that clarify the nature of itinerant ferromagnetism. This is because correlation effects are so strong that it is difficult to investigate it by conventional approaches such as perturbations from non-interacting systems.

In this way, strong electronic correlations sometimes cause non-trivial and interesting phenomena which are difficult to understand from the weak-coupling view-point. In order to extract fundamental aspects of interacting electron systems, it may be helpful to take the limit of strong correlation. As an example, let us consider the one-dimensional (1d) Hubbard model.

For the 1d Hubbard model, infinitesimal introduction of the interaction term (U-term) changes the low-energy physics[10]. For the repulsive case ($U > 0$), elementary excitations are characterized by spin

[1] In the mother compounds of high-T_c superconductors, antiferromagnetism is understood by the superexchange mechanism[4], which is due to kinetic exchange processes.

and charge gapless modes. This feature is usually referred to as spin-charge separation[11]. For the attractive case ($U < 0$), electrons form bound states. As a result, a spin gap opens. The 1d Hubbard model shows qualitatively the same low-energy properties in the parameter range $0 < U < +\infty$ for the repulsive case. (For the attractive case, $-\infty < U < 0$.) Essential features of the 1d Hubbard model are easily understood, if one considers the strong-correlation limit $U \to \infty$. For the repulsive case, in the limit $U \to +\infty$, spin and charge degrees of freedom are separated in the level of wavefunctions[12]. For the attractive case, in the limit $U \to -\infty$, electrons with opposite spins form bound states in the real space. In this way, by considering the limit of strong correlation, we can realize essential features of the 1d Hubbard model.

In this thesis, we take some limits in order to extract fundamental aspects of strongly correlated electron systems. This thesis consists of two parts: In part I, we consider the repulsive Hubbard model. In part II, the attractive Hubbard model with nearest neighbor repulsion is considered.

First, in part I, we derive the t-J model as the effective model of the $U \to +\infty$ Hubbard model. We review the Bethe ansatz results of the 1d Hubbard model in the limit $U \to +\infty$[12] to realize spin-charge separation in 1d electron systems. Next, we consider the Hubbard ladder as the simplest model in which some special features of the Hubbard chain are removed. We take $U = +\infty$, and investigate similarities and dissimilarities between ground-state properties of the Hubbard ladder and those of the Hubbard chain in the strong-coupling regime[13]. We present rigorous results in the limit of the large inter-chain hopping ($t_\perp/t \to \infty$). For finite $t_\perp/t$, we discuss ferromagnetism and the metal-insulator transition at quarter-filling based on the numerical results of the DMRG method. For comparison, ferromagnetism and the Mott transition in the two-dimensional t-J and Hubbard models are reviewed.

In part II, we consider the limit of the strong attractive interaction ($U \to -\infty$) of the Hubbard model with nearest neighbor repulsion. Generally, if attraction is strong enough, electrons form bound states. As a result, the effective models in this limit are boson models. First, we derive the spin-1/2 XXZ model with Ising-like anisotropy as the effective model of the $U \to -\infty$ Hubbard model with nearest neighbor

repulsion. We review the Bethe ansatz results of the spin-1/2 XXZ chain in the ground state[14], and discuss the magnetization process of it. Next, we investigate the magnetization process of the spin-1/2 XXZ models with Ising-like anisotropy on square and cubic lattices as an extreme case of the superconductor-insulator transition in the extended attractive Hubbard model[15]. By taking the limit of the strong nearest-neighbor repulsion, we demonstrate that quantum fluctuations drastically modify the doping dependence of the chemical potential for the extended attractive Hubbard model.

The outline of this thesis is shown in Fig. 1.1.

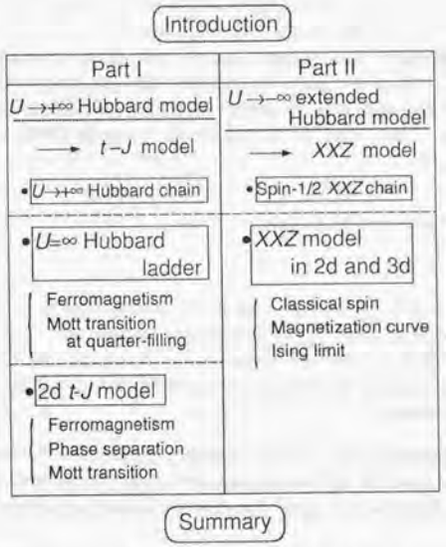

Figure 1.1: Outline of this thesis.

1.2 Hubbard model

In this thesis, we consider ground-state properties of effective models derived from the Hubbard-type models [2] in the strong coupling regime. The Hubbard model is defined by the following Hamiltonian:

$$\mathcal{H}_{\rm Hub} \equiv -t \sum_{\langle i,j \rangle \sigma} (c_{i\sigma}^{\dagger} c_{j\sigma} + \text{h.c.}) + U \sum_{i} (n_{i\uparrow} - 1/2)(n_{i\downarrow} - 1/2), \quad (1.1)$$

where $c_{i\sigma}^{\dagger}$ and $n_{i\sigma}$ denote the creation operator and the number operator of an electron with spin σ at site i, respectively. Here, $\langle i,j \rangle$ denotes nearest neighbors. Hereafter, the number of electrons and the number of sites are denoted by N_e and N_s, respectively.

In the following subsections, we refer to two theorems for the Hubbard model. One is Lieb's theorem[16] for the attractive Hubbard model and the repulsive Hubbard model at half-filling. The other is Nagaoka's theorem[7, 8, 9] for the $U = \infty$ Hubbard model with $N_e = N_s - 1$.

1.2.1 Lieb's theorem

Theorem 1.2.1 *(i) If U is negative, the ground state is unique and has total spin $S = 0$ for an even number of electrons. (ii) If U is positive and $N_e (= N_s)$ is even, the ground state is unique (up to the trivial $(2S+1)$-fold spin degeneracy) and has total spin $S = ||A| - |B||/2$ for a bipartite lattice.*

Here, a bipartite lattice means a lattice which can be divided into two sublattices A and B, and every non-zero t connects one of sites in A with one in B. Notation $|A|$ ($|B|$) denotes the number of sites in sublattice A (B).

For hyper-cubic lattices, this theorem ensures a spin-singlet ground state of the Hubbard model at half-filling with an even number of

[2] In Part II, we consider the effective model of the attractive Hubbard model with nearest neighbor repulsion.

electrons in finite-size clusters. This is naturally connected with the Marshall-Lieb-Mattis theorem for the Heisenberg model on bipartite lattices[17, 18].

1.2.2 Nagaoka's theorem

Theorem 1.2.2 *If the connectivity condition is satisfied, the ground state of the $U = \infty$ Hubbard model with $t < 0$ and $N_e = N_s - 1$ has the maximum total spin S $(= N_e/2)$ and is unique up to the trivial $(2S+1)$-fold degeneracy.*

The connectivity condition is the requirement that any configuration can be reached from any other configuration within the subspace of fixed total S^z after successive multiplication by the Hamiltonian. This condition holds for most of familiar lattice structures, except for the chain with nearest neighbor hopping.

For bipartite lattices, the requirement of $t < 0$ is replaced by $t \neq 0$, because the sign of t can be changed by the gauge transformation with spin operators unchanged.

Part I

Repulsive Hubbard model

Chapter 2

$U \to +\infty$ Hubbard model

2.1 Effective model up to order t^2/U

In this section, we consider the limit of the large repulsive interaction ($U \to +\infty$) of the Hubbard model defined in eq.(1.1).

Up to order t, the effective Hamiltonian is written as

$$\mathcal{H}_t^{\text{eff}} = -t \sum_{\langle i,j \rangle \sigma} (\tilde{c}_{i\sigma}^\dagger \tilde{c}_{j\sigma} + \text{h.c.}), \tag{2.1}$$

where $\tilde{c}_{i\sigma}^\dagger$ denotes the creation operator of an electron at site i with spin $\sigma(\sigma = \uparrow, \downarrow)$ with the constraint that no site is doubly occupied, or $\tilde{c}_{i\sigma}^\dagger \equiv c_{i\sigma}^\dagger (1 - n_{i-\sigma})$.

Next, we derive the effective Hamiltonian of order t^2/U. As shown in Fig. 2.1(a), electrons with opposite spins can sit on a site virtually, and go back to the initial positions or exchange their positions. This process is expressed by the following Hamiltonian:

$$\mathcal{H}_J^{\text{eff}(1)} = J \sum_{\langle i,j \rangle} (\boldsymbol{S}_i \cdot \boldsymbol{S}_j - \frac{1}{4} n_i n_j), \tag{2.2}$$

where $\boldsymbol{S}_i$ is the spin operator at site i, and $J = 4t^2/U$.

There is another process of order t^2/U. As shown in Fig. 2.1(b), an electron hops to next nearest neighbor sites if the spin on the nearest neighbor site is opposite, and the next nearest neighbor site is empty.

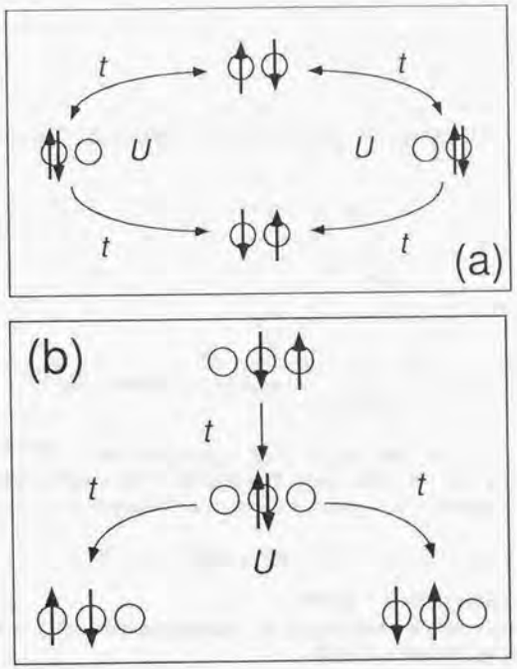

Figure 2.1: Second order perturbation of the repulsive Hubbard model in the large-U limit. (a) Exchange process. (b) Three-site process.

In this situation, the electron can also push the neighboring electron to the next nearest neighbor site. This three-site hopping process is expressed by the following Hamiltonian:

$$\mathcal{H}_J^{\mathrm{eff}(2)} = \frac{J}{4} \sum_{\langle\langle i,j,k\rangle\rangle, i\neq k, \sigma} (\tilde{c}_{i-\sigma}^\dagger \tilde{c}_{j\sigma}^\dagger \tilde{c}_{j-\sigma} \tilde{c}_{k\sigma} - \tilde{c}_{i\sigma}^\dagger n_{j-\sigma} \tilde{c}_{k\sigma} + \mathrm{h.c.}), \tag{2.3}$$

where $\langle\langle i,j,k\rangle\rangle$ denotes neighboring three-site groups.

Therefore, the effective Hamiltonian $\mathcal{H}^{\mathrm{eff}}$, up to order t^2/U, is obtained[19, 20, 21] as

$$\begin{aligned}
\mathcal{H}^{\mathrm{eff}} &= \mathcal{H}_t^{\mathrm{eff}} + \mathcal{H}_J^{\mathrm{eff}(1)} + \mathcal{H}_J^{\mathrm{eff}(2)}, \qquad (2.4)\\
\mathcal{H}_t^{\mathrm{eff}} &= -t \sum_{\langle i,j\rangle\sigma} (\tilde{c}_{i\sigma}^\dagger \tilde{c}_{j\sigma} + \mathrm{h.c.}),\\
\mathcal{H}_J^{\mathrm{eff}(1)} &= J \sum_{\langle i,j\rangle} (\boldsymbol{S}_i \cdot \boldsymbol{S}_j - \frac{1}{4} n_i n_j),\\
\mathcal{H}_J^{\mathrm{eff}(2)} &= \frac{J}{4} \sum_{\langle\langle i,j,k\rangle\rangle, i\neq k, \sigma} (\tilde{c}_{i-\sigma}^\dagger \tilde{c}_{j\sigma}^\dagger \tilde{c}_{j-\sigma} \tilde{c}_{k\sigma} - \tilde{c}_{i\sigma}^\dagger n_{j-\sigma} \tilde{c}_{k\sigma} + \mathrm{h.c.}).
\end{aligned}$$

At half-filling, the effective Hamiltonian reduces to $\mathcal{H}_J^{\mathrm{eff}(1)}$. This is nothing but the Heisenberg Hamiltonian. The doping effects are often discussed by investigating the system described by the following Hamiltonian:

$$\mathcal{H}_{tJ} \equiv \mathcal{H}_t^{\mathrm{eff}} + \mathcal{H}_J^{\mathrm{eff}(1)}. \tag{2.5}$$

This is called as the t-J model.

Another derivation of the t-J model, in relation to high-T_c cuprates, is shown in Appendix A.1[22].

2.2 $U \to +\infty$ Hubbard chain

As a first step to understand fundamental aspects of strongly correlated electron systems, we consider the one-dimensional (1d) Hubbard model. In this section, we review the Bethe ansatz results[10] for the $U \to +\infty$ Hubbard chain, following the paper by Ogata and Shiba[12].

The Hubbard chain is defined by the following Hamiltonian:

$$\mathcal{H} \equiv -t \sum_{i\sigma} (c_{i\sigma}^\dagger c_{i+1\sigma} + \mathrm{h.c.}) + U \sum_i n_{i\uparrow} n_{i\downarrow}. \tag{2.6}$$

Hereafter, N,M and L denote the number of electrons, the number of down spins and the length of a chain, respectively. We take $t = 1$ as the energy unit.

Let $f(x_1, \cdots, x_N)$ be the amplitude in the wavefunction when down spins are located at sites $x_1, \cdots, x_M$, and up spins at $x_{M+1}, \cdots, x_N$. Within each region of $x_{Q1} < x_{Q2} < \cdots < x_{QN}$, f is expressed under the Bethe ansatz as

$$f(x_1, \cdots, x_N) = \sum_P [Q, P] \exp(\mathrm{i} \sum_{j=1}^N k_{Pj} x_{Qj}), \tag{2.7}$$

where $P = (P1, P2, \cdots, PN)$ and $Q = (Q1, Q2, \cdots, QN)$ are two permutations of $(1, 2, \cdots, N)$. The coefficients $[Q, P]$ and quasi-momenta $(k_1, k_2, \cdots, k_N)$ are determined to satisfy the Schrödinger equation with the periodic boundary condition. The coefficients $[Q, P]$ should satisfy the relation

$$[Q, P] = Y_{nm}^{i,i+1} [Q, P'], \tag{2.8}$$

where

$$P = (P1, P2, \cdots, Pi = m, P(i+1) = n, \cdots, PN), \tag{2.9}$$

and

$$P' = (P1, P2, \cdots, n, m, \cdots, PN). \tag{2.10}$$

The operator $Y_{nm}^{i,i+1}$ is defined as

$$\begin{aligned}
Y_{nm}^{i,i+1} &\equiv (P_{i,i+1} - x_{nm})/(1 + x_{nm}), \qquad (2.11)\\
x_{nm} &\equiv \mathrm{i}(U/2)/(\sin k_n - \sin k_m), \qquad (2.12)
\end{aligned}$$

where $P_{i,i+1}$ is a permutation operator for the interchange between Q_i and Q_{i+1}. We can determine all $[Q, P]$'s from, for example, $[Q, P = \boldsymbol{I}]$. Here, $\boldsymbol{I}$ denotes the identity operator.

By imposing the periodic boundary condition, the coefficient $[Q, P = \boldsymbol{I}]$ and quasi-momenta k_j's are determined to satisfy the following equation:

$$
\begin{aligned}
e^{ik_jL}\chi(Q) &= X'_{j+1,j}\cdots X'_{N,j}X'_{1,j}\cdots X'_{j-1,j}\chi(Q), && (2.13)\\
\chi(Q) &\equiv (-1)^Q[Q, P = \boldsymbol{I}], && (2.14)\\
X'_{i,j} &\equiv (1 + x_{ij}P_{i,j})/(1 + x_{ij}), && (2.15)
\end{aligned}
$$

where $(-1)^Q$ is equal to -1 when Q is an odd permutation and 1 otherwise.

In order to express the spin degrees of freedom of χ, we introduce the "coordinates" of M down spins $(y_1, y_2, \cdots, y_M)$ in the spin configuration. For $y_1 < y_2 < \cdots < y_M$, the eigenvalue problem eq.(2.13) has been solved by Yang[23] with a generalized Bethe's hypothesis as

$$
\begin{aligned}
\chi &= \Phi(y_1, y_2, \cdots, y_M) && (2.16)\\
&= \sum_P A_P F(\Lambda_{P1}, y_1)F(\Lambda_{P2}, y_2)\cdots F(\Lambda_{PM}, y_M), && (2.17)
\end{aligned}
$$

where $F(\Lambda, y)$ and A_P are defined as

$$
\begin{aligned}
F(\Lambda, y) &\equiv \prod_{j=1}^{y-1}\frac{i\sin k_j - i\Lambda - U/4}{i\sin k_{j+1} - i\Lambda + U/4}, && (2.18)\\
A_P &\equiv (-1)^P\prod_{i<j}^{y-1}(\Lambda_{pi} - \Lambda_{pj} - iU/2). && (2.19)
\end{aligned}
$$

The quasi-momenta k_j's and rapidities Λ_α's are determined to satisfy the following equations:

$$
\begin{aligned}
\prod_j \frac{i\sin k_j - i\Lambda_\alpha - U/4}{i\sin k_j - i\Lambda_\alpha + U/4} &= -\prod_\beta \frac{-i\Lambda_\beta + i\Lambda_\alpha + U/2}{-i\Lambda_\beta + i\Lambda_\alpha - U/2}, && (2.20)\\
e^{ik_jL} &= \prod_\alpha \frac{i\sin k_j - i\Lambda_\alpha - U/4}{i\sin k_j - i\Lambda_\alpha + U/4}. && (2.21)
\end{aligned}
$$

The above equations are simplified, when we take the limit $U \to \infty$. We neglect $\sin k_j$'s$(= O(1))$ which is much smaller than $U(\gg 1)$. Thus, the distribution of rapidities Λ_α's are determined by eq.(2.20),

which corresponds to the Bethe-ansatz equation for the one-dimensional Heisenberg model[24]. The quasi-momenta k_j's are determined by eq.(2.21), which leads to

$$
\begin{aligned}
k_jL &= 2\pi I_j - \sum_\alpha \theta(2\Lambda_\alpha) && (2.22)\\
&= 2\pi(I_j + \frac{1}{N}\sum_\alpha J_\alpha), && (2.23)
\end{aligned}
$$

where

$$
\theta(p) \equiv -2\tan^{-1}(2p/U), \qquad (2.24)
$$

and

$$
\begin{aligned}
I_j &= \begin{cases} \text{integer for } M \text{ even,} \\ \text{half-odd integer for } M \text{ odd,} \end{cases} && (2.25)\\
J_\alpha &= \begin{cases} \text{integer for } N - M \text{ odd,} \\ \text{half-odd integer for } N - M \text{ even.} \end{cases} && (2.26)
\end{aligned}
$$

The coefficients $[Q, P]$'s determined by eq.(2.8) are simplified by taking the limit $U \to \infty$, because, in this limit, the operator Y reduces to -1. Thus, $[Q, P]$'s are obtained as

$$
[Q, P] = (-1)^P[Q, P = \boldsymbol{I}]. \qquad (2.27)
$$

Hence, in the limit $U \to \infty$, the amplitude in the wavefunction $f(x_1, \cdots, x_N)$ is obtained as

$$
\begin{aligned}
f(x_1, \cdots, x_N) &= \sum_P (-1)^P(-1)^Q\Phi(y_1, \cdots, y_M)\exp(i\sum_{i=1}^N k_{Pj}x_{Qj})\\
&= (-1)^Q\det[\exp(i\sum_{i=1}^N k_{Pj}x_{Qj})]\Phi(y_1, \cdots, y_M). && (2.28)
\end{aligned}
$$

The determinant depends on the positions of the particles $(x_1, \cdots, x_N)$ but not on their spins. Thus, it is the same as the Slater determinant of spinless fermions with momenta k_j's. The wavefunction $\Phi(y_1, \cdots, y_M)$ corresponds to the Bethe-ansatz wavefunction for the one-dimensional Heisenberg model[24]. Hence, the wavefunction of the one-dimensional Hubbard model in the limit $U \to \infty$ is divided into the charge part

(the Slater determinant of spinless fermions) and the spin part (the wavefunction of the Heisenberg model).

For $U = \infty$, the ground states are degenerate with respect to the spin degrees of freedom. However, in the limit $U \to \infty$, the ground state is a spin-singlet in the following cases, (i) $N = 4m + 2$ with the periodic boundary condition, (ii) $N = 4m$ with the anti-periodic boundary condition, where m is an integer. Hence, the perturbation of order t^2/U removes the degeneracy with respect to the spin degrees of freedom and selects a spin-singlet state as the ground state under appropriate boundary conditions.

Chapter 3

$U = \infty$ Hubbard ladder

3.1 Introduction

In Sec. 2.2, we have seen that the one-dimensional (1d) Hubbard model in the limit $U \to +\infty$ exhibits spin-charge separation in the level of wavefunctions, and that the ground state is a spin singlet with appropriate boundary conditions. One might ask whether these features are special to single chain models, or common in strongly correlated electron systems.

First, let us consider the possibility of itinerant ferromagnetism in the Hubbard model. Itinerant ferromagnetism is one of the phenomena which have not been fully understood yet. Hund's coupling due to orbital degeneracy probably works for enhancement of ferromagnetic correlations in real materials. However, there is a possibility that, without orbital degeneracy, ferromagnetism is caused by purely electronic correlations. Nagaoka's theorem states that, except for one dimension, the ground state of the $U = \infty$ Hubbard model is ferromagnetic, if the number of holes is one[7, 8, 9]. (See subsection 1.2.2.) A naive expectation is that the ground state of Hubbard-type models with finite hole-doping near half-filling may be ferromagnetic, if the repulsive interaction is strong enough. To make the argument simpler, let us consider the $U = \infty$ Hubbard model with nearest-neighbor hopping on bipartite lattices. The simplest case is the $U = \infty$ Hubbard chain. In this case, as shown in Sec. 2.2, the ground states are degenerate with

respect to the spin degrees of freedom. The energy is determined only by the charge distribution, regardless of spin configurations.[1] Infinitesimal perturbation of order t^2/U removes the degeneracy and selects a spin-singlet state. Thus, for the Hubbard chain, ferromagnetism is not realized. Actually, it is rigorously proved, by Lieb and Mattis, that the ground state of the one-dimensional Hubbard model cannot be ferromagnetic under the open boundary condition[25]. As for two and three dimensions, a lot of attempts have been made in order to clarify the mechanism of itinerant ferromagnetism from the electron-correlation view-point[26, 27, 28, 29, 30, 31, 32, 33, 34]. (See Sec. 4.2 for a detailed review.) In spite of many such attempts, results are inconclusive. One of the reasons is a lack of efficient methods. For example, Monte Carlo simulations suffer from a severe negative sign problem. Exact diagonalization is also difficult to deduce properties in the thermodynamic limit, because system sizes are restricted up to about 20 sites.

In this chapter, we mainly consider the $U = \infty$ Hubbard ladder. One of the reasons is that the $U = \infty$ Hubbard ladder is the simplest model on a bipartite lattice that Nagaoka's theorem holds for. Another reason is that there is an efficient method to investigate ground-state properties of quasi-one dimensional systems, i.e. the density-matrix renormalization group (DMRG) method proposed by White[35]. Liang and Pang applied this method to the $U = \infty$ Hubbard ladder for $t_\perp/t = 1$, and obtained some indications of ferromagnetism[34]. As for the (two-leg) ladder, the DMRG calculation in Ref.[34] suggests that the fully-polarized ferromagnetic state is one of the ground states for $\delta < 0.22$ (δ : hole density), and that the ground state is a spin-singlet for $\delta \gtrsim 0.4$. They have tried to extend these results to two dimensions by investigating multi-leg ladders. In this chapter, we extend their results to various values of $t_\perp$ and J for the t-J ladder, in order to understand the ground-state properties of the Hubbard and t-J ladders in the strong-coupling regime.

The $U = \infty$ Hubbard ladder (or t-ladder) is defined as the t-J ladder for $J = J_\perp = 0$. (Later, in Sec. 3.3, we briefly discuss ferromagnetism in the t-J ladder.) The Hamiltonian of the t-J ladder is defined as

[1] Actually, Nagaoka's theorem dose not hold for the Hubbard chain.

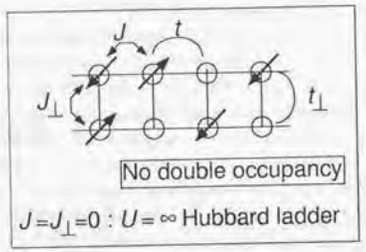

Figure 3.1: t-J ladder.

follows:

$$
\begin{aligned}
\mathcal{H}_{tJ} &= \mathcal{H}_t + \mathcal{H}_J, \qquad (3.1)\\
\mathcal{H}_t &= -t\sum_{i\sigma}(\tilde{c}^{1\dagger}_{i\sigma}\tilde{c}^{1}_{i+1\sigma} + \tilde{c}^{2\dagger}_{i\sigma}\tilde{c}^{2}_{i+1\sigma} + \text{h.c.})\\
&\quad -t_\perp\sum_{i\sigma}(\tilde{c}^{1\dagger}_{i\sigma}\tilde{c}^{2}_{i\sigma} + \text{h.c.}),\\
\mathcal{H}_J &= J\sum_i(\boldsymbol{S}^1_i\cdot\boldsymbol{S}^1_{i+1} - \frac{1}{4}n^1_i n^1_{i+1} + \boldsymbol{S}^2_i\cdot\boldsymbol{S}^2_{i+1} - \frac{1}{4}n^2_i n^2_{i+1})\\
&\quad +J_\perp\sum_i(\boldsymbol{S}^1_i\cdot\boldsymbol{S}^2_i - \frac{1}{4}n^1_i n^2_i),
\end{aligned}
$$

where $\tilde{c}^{\alpha\dagger}_{i\sigma}$ denotes a creation operator of an electron at rung i with spin $\sigma(\sigma=\uparrow,\downarrow)$ in the α-th chain ($\alpha=1,2$) with the constraint that no site is doubly occupied, i.e. $\tilde{c}^{\alpha\dagger}_{i\sigma}\equiv c^{\alpha\dagger}_{i\sigma}(1-n^{\alpha}_{i-\sigma})$. The number operator $n^{\alpha}_{i\sigma}$ is defined as $n^{\alpha}_{i\sigma}\equiv c^{\alpha\dagger}_{i\sigma}c^{\alpha}_{i\sigma}$, using the standard electron creation operator $c^{\alpha\dagger}_{i\sigma}$. The spin operator at rung i in the α-th chain is defined as $\boldsymbol{S}^{\alpha}_i\equiv\frac{1}{2}\sum_{\beta\gamma}c^{\alpha\dagger}_{i\beta}\boldsymbol{\sigma}_{\beta\gamma}c^{\alpha}_{i\gamma}$, where $\boldsymbol{\sigma}$ is the vector of Pauli matrices. The number of electrons, the number of sites and the number of rungs are denoted by N_e, N_s and $L(=N_s/2)$, respectively. The electron density n and the hole density δ are defined as $n\equiv N_e/N_s$ and $\delta\equiv 1-n$, respectively. The maximum value of the total spin S is denoted by $S_{\max}(=N_e/2)$.

This chapter is organized as follows: In Sec. 3.2, we present rigorous results on the ground state of the t-ladder in the limit $t_\perp/t\to\infty$. In Sec. 3.3, we present numerical results on ferromagnetism in the t-ladder and the t-J ladder. In Sec. 3.4, we discuss the metal-insulator transition at quarter-filling in the Hubbard ladder. Section 3.5 is a summary.

3.2 $t_\perp/t\to\infty$ limit for the $U=\infty$ Hubbard ladder

As a first step, let us consider the limit of the large inter-chain hopping ($t_\perp/t\to\infty$) of the $U=\infty$ Hubbard ladder. In this section, we prove the following statements:

1. The ground state of the t-ladder in the limit $t_\perp/t\to\infty$ up to order $t^2/t_\perp$ for $n\le 0.5$ is a spin-singlet ($S=0$) and is unique in finite-size clusters with an even number of electrons with open boundary conditions.

2. The ground state of the t-ladder in the limit $t_\perp/t\to\infty$ up to order t for $n>0.5$ has the maximum total spin ($S=S_{\max}$) and is unique up to the trivial $(2S+1)$-fold degeneracy in finite-size clusters with open boundary conditions.

Before referring to the above statements, we consider the t-ladder for $t=0$. The ground states of this model can be written in the following form:

$$|\Phi\rangle=\bigotimes_{i=1}^{L}|\alpha\rangle_i, \qquad (3.2)$$

where $|\alpha\rangle_i$'s correspond to either of states (i)-(iii) defined in table 3.1 for $n\le 0.5$, and (ii)-(vii) for $n>0.5$. The degeneracy of the ground states, the energy E and the chemical potential $\mu(\equiv\partial E/\partial N_e)$ are summarized in table 3.2. The charge gap Δ_c at quarter-filling ($n=0.5$) is $2t_\perp$.

Next, we consider the t-ladder in the limit $t/t_\perp\to 0$. Let us consider the cases $n\le 0.5$ and $n>0.5$, separately.

Table 3.1: Basis set.

	Symbol	Definition	Energy
(i)	$\|00\rangle_i$	vacuum	0
(ii)	$\|B\uparrow\rangle_i$	$\frac{1}{\sqrt{2}}(\tilde{c}_{i\uparrow}^{1\dagger} + \tilde{c}_{i\uparrow}^{2\dagger})\|00\rangle_i$	$-t_\perp$
(iii)	$\|B\downarrow\rangle_i$	$\frac{1}{\sqrt{2}}(\tilde{c}_{i\downarrow}^{1\dagger} + \tilde{c}_{i\downarrow}^{2\dagger})\|00\rangle_i$	$-t_\perp$
(iv)	$\|\uparrow\uparrow\rangle_i$	$\tilde{c}_{i\uparrow}^{1\dagger}\tilde{c}_{i\uparrow}^{2\dagger}\|00\rangle_i$	0
(v)	$\|\downarrow\downarrow\rangle_i$	$\tilde{c}_{i\downarrow}^{1\dagger}\tilde{c}_{i\downarrow}^{2\dagger}\|00\rangle_i$	0
(vi)	$\|\uparrow\downarrow\rangle_i$	$\tilde{c}_{i\uparrow}^{1\dagger}\tilde{c}_{i\downarrow}^{2\dagger}\|00\rangle_i$	0
(vii)	$\|\downarrow\uparrow\rangle_i$	$\tilde{c}_{i\downarrow}^{1\dagger}\tilde{c}_{i\uparrow}^{2\dagger}\|00\rangle_i$	0

Table 3.2: Ground states at $t = 0$.

	$n < 0.5$	$0.5 < n < 1$
Degeneracy	${}_L C_{N_e} \times 2^{N_e}$	${}_L C_{N_e - L} \times 2^{N_e}$
Energy E	$-t_\perp \times N_e$	$-t_\perp \times (2L - N_e)$
Chemical Potential μ	$-t_\perp$	$t_\perp$

Table 3.3: Second-order perturbation energy E_2.

E_2 between $\|\alpha\rangle$ and $\|\beta\rangle$	$\|\alpha\rangle$	$\|\beta\rangle$
0	$\|B\sigma\rangle_i \otimes \|B\sigma\rangle_{i+1}$	$\|B\sigma\rangle_i \otimes \|B\sigma\rangle_{i+1}$
$-t^2/(2t_\perp)$	$\|B\sigma\rangle_i \otimes \|B-\sigma\rangle_{i+1}$	$\|B\sigma\rangle_i \otimes \|B-\sigma\rangle_{i+1}$
$t^2/(2t_\perp)$	$\|B\sigma\rangle_i \otimes \|B-\sigma\rangle_{i+1}$	$\|B-\sigma\rangle_i \otimes \|B\sigma\rangle_{i+1}$
$t^2/(4t_\perp)$	$\|00\rangle_{i-1} \otimes \|B\sigma\rangle_i \otimes \|B-\sigma\rangle_{i+1}$	$\|B\sigma\rangle_i \otimes \|B-\sigma\rangle_i \otimes \|00\rangle_{i+1}$
$-t^2/(4t_\perp)$	$\|00\rangle_{i-1} \otimes \|B\sigma\rangle_i \otimes \|B-\sigma\rangle_{i+1}$	$\|B-\sigma\rangle_i \otimes \|B\sigma\rangle_i \otimes \|00\rangle_{i+1}$

3.2.1 $n \leq 0.5$

In this subsection, we consider the case $n \leq 0.5$. In the limit $t/t_\perp \to 0$, up to order t, the effective Hamiltonian is written as

$$\mathcal{H}_t^{\rm eff} = -t \sum_{i\sigma} (\tilde{b}_{i\sigma}^\dagger \tilde{b}_{i+1\sigma} + \text{h.c.}), \tag{3.3}$$

where $\tilde{b}_{i\sigma}^\dagger$ denotes a creation operator of an electron in the bonding band at rung i with spin $\sigma(\sigma = \uparrow, \downarrow)$ with the constraint that no rung is doubly occupied, or $\tilde{b}_{i\sigma}^\dagger \equiv b_{i\sigma}^\dagger(1 - n_i^1 - n_i^2)$. Here, the creation operator $b_{i\sigma}^\dagger$ is defined as $b_{i\sigma}^\dagger \equiv (\tilde{c}_{i\sigma}^{1\dagger} + \tilde{c}_{i\sigma}^{2\dagger})/\sqrt{2}$. This Hamiltonian is equivalent to the $U = \infty$ Hubbard chain. Thus, the ground states are degenerate with respect to the spin degrees of freedom. The charge part of the ground-state wavefunction is simply that of the spinless fermion model on a chain.

Next, we consider the effective Hamiltonian of order $t^2/t_\perp$. Here, we define the local Hamiltonian $\mathcal{H}_{i,i+1\sigma}^{\rm loc}$:

$$\mathcal{H}_{i,i+1\sigma}^{\rm loc} \equiv -t(\tilde{c}_{i\sigma}^{1\dagger}\tilde{c}_{i+1\sigma}^{1} + \tilde{c}_{i\sigma}^{2\dagger}\tilde{c}_{i+1\sigma}^{2} + \text{h.c.}). \tag{3.4}$$

Letting this local Hamiltonian operate on $|\alpha\rangle_i \otimes |\beta\rangle_{i+1}$, we obtain the following relations:

$$\begin{aligned}
\mathcal{H}_{i,i+1\sigma}^{\rm loc}|B\sigma\rangle_i \otimes |B\sigma\rangle_{i+1} &= 0, \\
\mathcal{H}_{i,i+1\sigma}^{\rm loc}|B-\sigma\rangle_i \otimes |B\sigma\rangle_{i+1} &= \frac{\sigma t}{\sqrt{2}}|S\rangle_i \otimes |00\rangle_{i+1}, \\
\mathcal{H}_{i,i+1\sigma}^{\rm loc}|B\sigma\rangle_i \otimes |B-\sigma\rangle_{i+1} &= -\frac{\sigma t}{\sqrt{2}}|00\rangle_i \otimes |S\rangle_{i+1},
\end{aligned}$$

$$\begin{aligned}
\mathcal{H}^{\rm loc}_{i,i+1\sigma}|S\rangle_i \otimes |00\rangle_{i+1} &= \frac{\sigma t}{\sqrt{2}}(|B-\sigma\rangle_i \otimes |B\sigma\rangle_{i+1} - |A-\sigma\rangle_i \otimes |A\sigma\rangle_{i+1}),\\
\mathcal{H}^{\rm loc}_{i,i+1\sigma}|00\rangle_i \otimes |S\rangle_{i+1} &= -\frac{\sigma t}{\sqrt{2}}(|B\sigma\rangle_i \otimes |B-\sigma\rangle_{i+1} - |A\sigma\rangle_i \otimes |A-\sigma\rangle_{i+1}),
\end{aligned}$$

where $|S\rangle_i$ and $|A\sigma\rangle_i$ are defined as $\frac{1}{\sqrt{2}}(\tilde{c}^{1\dagger}_{i\uparrow}\tilde{c}^{2\dagger}_{i\downarrow} - \tilde{c}^{1\dagger}_{i\downarrow}\tilde{c}^{2\dagger}_{i\uparrow})|00\rangle_i$ and $\frac{1}{\sqrt{2}}(\tilde{c}^{1\dagger}_{i\sigma} - \tilde{c}^{2\dagger}_{i\sigma})|00\rangle_i$, respectively. Thus, the second-order perturbation energy E_2 is obtained as in table 3.3. It is also shown that the following relations are satisfied:

$$\begin{aligned}
n^B_{i\uparrow}n^B_{i+1\downarrow}|B\uparrow\rangle_i \otimes |B\downarrow\rangle_{i+1} &= |B\uparrow\rangle_i \otimes |B\downarrow\rangle_{i+1},\\
S^{B-}_i S^{B+}_{i+1}|B\uparrow\rangle_i \otimes |B\downarrow\rangle_{i+1} &= |B\downarrow\rangle_i \otimes |B\uparrow\rangle_{i+1},
\end{aligned}$$

where $S^{B+}_i \equiv \tilde{b}^\dagger_{i\uparrow}\tilde{b}_{i\downarrow}$ and $n^B_{i\sigma} \equiv \tilde{b}^\dagger_{i\sigma}\tilde{b}_{i\sigma}$. Thus, the effective Hamiltonian $\mathcal{H}^{\rm eff}$, up to order $t^2/t_\perp$, is written as follows:

$$\begin{aligned}
\mathcal{H}^{\rm eff} &= \mathcal{H}^{\rm eff}_t + \mathcal{H}^{\rm eff(1)}_J + \mathcal{H}^{\rm eff(2)}_J, \qquad (3.5)\\
\mathcal{H}^{\rm eff(1)}_J &= J_{\rm eff}\sum_i(\boldsymbol{S}^B_i \cdot \boldsymbol{S}^B_{i+1} - \frac{1}{4}n^B_i n^B_{i+1}),\\
\mathcal{H}^{\rm eff(2)}_J &= \frac{J_{\rm eff}}{4}\sum_{i\sigma}(\tilde{b}^\dagger_{i-1-\sigma}\tilde{b}^\dagger_{i\sigma}\tilde{b}_{i-\sigma}\tilde{b}_{i+1\sigma} - \tilde{b}^\dagger_{i-1\sigma}n^B_{i-\sigma}\tilde{b}_{i+1\sigma} + \text{h.c.}),
\end{aligned}$$

where $\boldsymbol{S}^B_i$ is the spin operator in the bonding band at rung i, and $J_{\rm eff} = t^2/t_\perp$. Hence, it is shown that the effective Hamiltonian, up to order $t^2/t_\perp$ for $n \le 0.5$, has the same form as that of the $U \to \infty$ Hubbard chain, up to order t^2/U for $n \le 1$[19, 20, 21, 12]. As a result, the ground-state properties of the t-ladder in the limit $t_\perp/t \to \infty$ for $n \le 0.5$ are the same as those of the $U \to \infty$ Hubbard chain for $n \le 1$[12]. This leads to a spin-singlet ground state by the Lieb-Mattis theorem[25].

3.2.2 $n > 0.5$

In this subsection, we consider the case $n > 0.5$. The unperturbed ground states are written in the form of eq.(3.2). The matrix elements of the local Hamiltonian eq.(3.6) are summarized in table 3.4.

$$\mathcal{H}^{\rm loc}_{i,i+1} \equiv -t\sum_\sigma(\tilde{c}^{1\dagger}_{i\sigma}\tilde{c}^1_{i+1\sigma} + \tilde{c}^{2\dagger}_{i\sigma}\tilde{c}^2_{i+1\sigma} + \text{h.c.}). \qquad (3.6)$$

Table 3.4: Matrix elements.

$\langle\alpha\|\mathcal{H}^{\rm loc}_{i,i+1}\|\beta\rangle$	$\|\alpha\rangle$	$\|\beta\rangle$
t	$\|B\sigma\rangle_i \otimes \|\sigma\sigma\rangle_{i+1}$	$\|\sigma\sigma\rangle_i \otimes \|B\sigma\rangle_{i+1}$
$t/2$	$\|B\sigma\rangle_i \otimes \|\sigma-\sigma\rangle_{i+1}$	$\|\sigma-\sigma\rangle_i \otimes \|B\sigma\rangle_{i+1}$
	$\|B\sigma\rangle_i \otimes \|\sigma-\sigma\rangle_{i+1}$	$\|\sigma\sigma\rangle_i \otimes \|B-\sigma\rangle_{i+1}$
	$\|B\sigma\rangle_i \otimes \|-\sigma\sigma\rangle_{i+1}$	$\|-\sigma\sigma\rangle_i \otimes \|B\sigma\rangle_{i+1}$
	$\|B\sigma\rangle_i \otimes \|-\sigma\sigma\rangle_{i+1}$	$\|\sigma\sigma\rangle_i \otimes \|B-\sigma\rangle_{i+1}$
	$\|B\sigma\rangle_i \otimes \|-\sigma-\sigma\rangle_{i+1}$	$\|-\sigma\sigma\rangle_i \otimes \|B-\sigma\rangle_{i+1}$
	$\|B\sigma\rangle_i \otimes \|-\sigma-\sigma\rangle_{i+1}$	$\|\sigma-\sigma\rangle_i \otimes \|B-\sigma\rangle_{i+1}$
0	otherwise	

Considering the matrix elements in table 3.4, we can show that the state $|B-\sigma\rangle_i \otimes |\sigma\sigma\rangle_{i+1}$ can reach the state $|\sigma\sigma\rangle_i \otimes |B-\sigma\rangle_{i+1}$ after successive multiplication by the local Hamiltonian $\mathcal{H}^{\rm loc}_{i,i+1}$ as follows: $|B-\sigma\rangle_i \otimes |\sigma\sigma\rangle_{i+1} \to |\sigma-\sigma\rangle_i \otimes |B\sigma\rangle_{i+1} \to |B\sigma\rangle_i \otimes |\sigma-\sigma\rangle_{i+1} \to |\sigma\sigma\rangle_i \otimes |B-\sigma\rangle_{i+1}$. Using this property, we can show that the following processes are possible by applying the local Hamiltonians $\mathcal{H}^{\rm loc}_{i-1,i}$ and $\mathcal{H}^{\rm loc}_{i,i+1}$ successively.

$$\begin{aligned}
|B\sigma\rangle_{i-1} \otimes |\sigma\sigma\rangle_i \otimes |\sigma-\sigma\rangle_{i+1} &\leftrightarrow |B\sigma\rangle_{i-1} \otimes |\sigma-\sigma\rangle_i \otimes |\sigma\sigma\rangle_{i+1},\\
|B\sigma\rangle_{i-1} \otimes |\sigma\sigma\rangle_i \otimes |-\sigma\sigma\rangle_{i+1} &\leftrightarrow |B\sigma\rangle_{i-1} \otimes |-\sigma\sigma\rangle_i \otimes |\sigma\sigma\rangle_{i+1},\\
|B\sigma\rangle_{i-1} \otimes |-\sigma-\sigma\rangle_i \otimes |-\sigma\sigma\rangle_{i+1} &\leftrightarrow |B\sigma\rangle_{i-1} \otimes |-\sigma\sigma\rangle_i \otimes |-\sigma-\sigma\rangle_{i+1},\\
|B\sigma\rangle_{i-1} \otimes |-\sigma-\sigma\rangle_i \otimes |\sigma-\sigma\rangle_{i+1} &\leftrightarrow |B\sigma\rangle_{i-1} \otimes |\sigma-\sigma\rangle_i \otimes |-\sigma-\sigma\rangle_{i+1},\\
|B\sigma\rangle_{i-1} \otimes |\sigma\sigma\rangle_i \otimes |-\sigma-\sigma\rangle_{i+1} &\leftrightarrow |B\sigma\rangle_{i-1} \otimes |-\sigma-\sigma\rangle_i \otimes |\sigma\sigma\rangle_{i+1},\\
|B\sigma\rangle_{i-1} \otimes |\sigma-\sigma\rangle_i \otimes |-\sigma\sigma\rangle_{i+1} &\leftrightarrow |B\sigma\rangle_{i-1} \otimes |-\sigma\sigma\rangle_i \otimes |\sigma-\sigma\rangle_{i+1}.
\end{aligned}$$

Thus, $|\uparrow\uparrow\rangle$, $|\uparrow\downarrow\rangle$, $|\downarrow\uparrow\rangle$ and $|\downarrow\downarrow\rangle$ can have their positions changed after successive multiplication by the Hamiltonian ($\mathcal{H}_t$), if there exists at least one $|B\uparrow\rangle$ or $|B\downarrow\rangle$. Furthermore, the following processes are also possible:

$$\begin{aligned}
|\sigma\sigma\rangle_{i-1} \otimes |B\sigma\rangle_i \otimes |B-\sigma\rangle_{i+1} &\leftrightarrow |\sigma\sigma\rangle_{i-1} \otimes |B-\sigma\rangle_i \otimes |B\sigma\rangle_{i+1},\\
|\sigma-\sigma\rangle_{i-1} \otimes |B\sigma\rangle_i \otimes |B-\sigma\rangle_{i+1} &\leftrightarrow |\sigma-\sigma\rangle_{i-1} \otimes |B-\sigma\rangle_i \otimes |B\sigma\rangle_{i+1}.
\end{aligned}$$

Thus, $|B\uparrow\rangle$ and $|B\downarrow\rangle$ can have their positions changed, if there exists at least one $|\uparrow\uparrow\rangle$, $|\uparrow\downarrow\rangle$, $|\downarrow\uparrow\rangle$ or $|\downarrow\downarrow\rangle$. As a result, any unperturbed

ground state in the form of eq.(3.2) can be reached after successive multiplication by the Hamiltonian ($\mathcal{H}_t$) for $0.5 < n < 1$ in the subspace of fixed total S^z and fixed electron number. This property is usually called connectivity. Owing to this property and the fact that the matrix elements of the Hamiltonian in this representation are not negative (table 3.4), the Perron-Frobenius theorem ensures that the state of the largest eigenvalue is unique and the wavefunction is positive (nodeless) in this representation in each subspace.

Next, we consider the ground-state wavefunction in the subspace of the maximum total S^z ($S^z = S_{\max}$). The Hamiltonian in this subspace has the same form as that of the spinless fermion model on a chain. Thus, the wavefunction of the largest eigenvalue in this subspace is nothing but that of the spinless fermion model ($|\Psi_{\rm SF}\rangle$). Applying the spin-lowering operator S^- to $|\Psi_{\rm SF}\rangle$, we obtain the eigenstates of various total S^z's. These states have all positive (nodeless) wavefunctions in the present representation. Thus, these states have finite overlap with the states of the largest eigenvalue in the corresponding subspaces. By use of the gauge transformation $\tilde{c}_i^\sigma \to (-1)^i \tilde{c}_i^\sigma, \sigma = 1, 2$, the sign of the hopping amplitude t can be changed as $t \to -t$, with spin operators unchanged. As a result, it is shown that the ground state of the t-ladder in the limit $t_\perp/t \to \infty$ up to order t for $0.5 < n < 1$ has the maximum total spin ($S = S_{\max}$) and is unique up to the trivial $(2S+1)$-fold degeneracy.

3.2.3 Remarks

Here, we give some remarks.

1. Part of theorem 1 can be extended to higher dimensions. The effective Hamiltonian of double-layer t-models up to order $t^2/t_\perp$ for $n \leq 0.5$ has the same form as that of the single-layer Hubbard models up to order t^2/U for $n \leq 1$[19, 20, 21]. Thus, the ground-state properties of double-layer t-models in the limit $t_\perp/t \to \infty$ for $n \leq 0.5$ are the same as those of the single-layer $U \to \infty$ Hubbard models for $n \leq 1$[16].

2. The proof of theorem 2 is mathematically similar to that of Kubo's theorem[36]. However, the physical situation is different. In Kubo's theorem, the limit of the strong Hund-coupling is taken, i.e. $H_{\rm Hund} \equiv -J_{\rm H} \sum_i \boldsymbol{S}_i^1 \cdot \boldsymbol{S}_i^2$, $J_{\rm H} \to \infty$. Furthermore, almost degenerate bands are assumed. On the other hand, in theorem 2, we do not assume explicit ferromagnetic couplings. In contrast to Kubo's case, the limit of the large band splitting is taken in the present case. The extension of Kubo's theorem to $n \leq 0.5$ shows that the ground state is also ferromagnetic[37], which is contrasted with theorem 1. The proof of theorem 2 is mathematically similar to that of Ref.[38] for the one-dimensional Kondo-lattice model, too.

3. The restriction on the boundary condition can be relaxed such that the Hubbard chain has a unique spin-singlet ground state for theorem 1 and that the spinless fermion model on a chain has no negative matrix elements in the site representation for theorem 2. For example, theorem 2 can be extended to the case of periodic boundary conditions with an odd number of electrons and an even number of rungs. Nagaoka's theorem is recovered for the one-hole case[7, 8, 9]

3.3 Ferromagnetism in the t-J ladder

In the previous section, we have shown rigorously, in a perturbative sense, that the ground-state of the $U = \infty$ Hubbard ladder in the limit $t_\perp/t \to \infty$ is ferromagnetic for $n > 0.5$. One might ask whether this ferromagnetic state survives for finite $t_\perp$, J and $J_\perp$ of the t-J ladder. Thus, in this section, we present the numerical results on the t-ladder for finite $t_\perp/t$ and the t-J ladder for small J and $J_\perp$ obtained by the DMRG method (finite-size algorithm)[35]. The DMRG calculation has been performed with open boundary conditions.

As a test of the DMRG calculation, we compare the ground-state energy obtained by the DMRG method with that of the exact diagonalization method. In Fig. 3.2, the agreement of the data obtained by these two methods is good. The maximum error is about 0.01%. Next, we consider the truncation error, i.e. the error due to small m, where m is the number of states kept in the superblock[35]. The difference

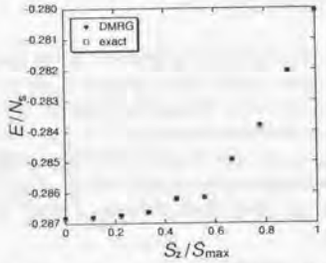

Figure 3.2: Energy per site as a function of the total S^z, measured from that of $S^z = S_{\max}$, for the t-J ladder at $J = J_\perp = 0.05$ and $t = t_\perp = 1$ in a 10×2-site cluster with 18 electrons. The solid diamonds and open squares correspond to the data obtained by the DMRG method and the exact diagonalization method, respectively. For the DMRG method, we took $m = 50$ (m : the number of states kept in the superblock[35]) and repeated 2-3 sweeps for convergence.

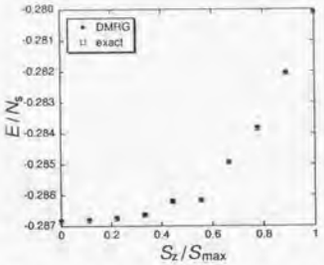

Figure 3.3: Energy difference $\Delta E_{\rm F}$ per site between the ground-state energy in the subspace of $S^z = 0$ and that of $S^z = S_{\max}$ as a function of filling for the t-ladder at $t_\perp/t = 1$. The solid diamonds and open squares correspond to the data of $m = 50$ and $m = 100$, respectively. $t = 1$.

between $m = 50$ and $m = 100$ is very small as shown in Fig. 3.3, suggesting that $m = 50$ is sufficient. (See also Fig. 3.5.) Thus, we mainly report the results of $m = 50$ hereafter.

Let us consider ferromagnetism of the t-ladder. In Fig. 3.4, we show the energy difference $\Delta E_{\rm F}$ between the ground-state energy in the subspace of $S^z = 0$ and that of $S^z = S_{\max}$ as a function of filling. The data in various-size clusters are scaled to a single line, indicating that the finite-size error is small. (See also Fig. 3.8.) From this plot, we find the region FF where the fully-polarized ferromagnetic state is one of the ground states. The phase boundary n_{c_1} between FF and non-FF is estimated as shown in Fig. 3.12. At $t_\perp/t = 1$, the result in Ref.[34] ($n_{c_1} \simeq 0.78$) is recovered. Qualitatively, the region FF becomes larger as $t_\perp/t$ increases. The phase boundary n_{c_1} gets closer to 0.5 as $t_\perp/t$ increases. This is consistent with the rigorous results in Sec. 3.2.

Next, we consider the phase boundary n_{c_2} between SS and non-SS, where SS is defined as the region in which the ground state is a spin-singlet. Figure 3.5 shows the ground-state energy as a function of the total S^z at $t_\perp/t = 1$ for $n = 0.5625$, 0.625 and 0.6875. The ground

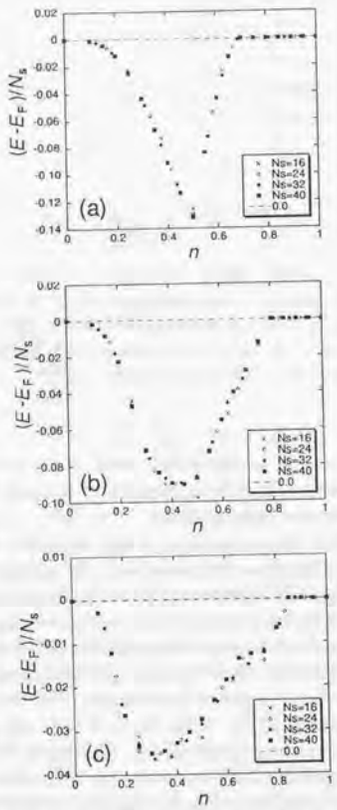

Figure 3.4: Energy difference $\Delta E_{\rm F}$ per site as a function of filling for the t-ladder at $t_\perp/t$ =2.5 [(a)], 1.0 [(b)] and 0.5 [(c)]. $t = 1$.

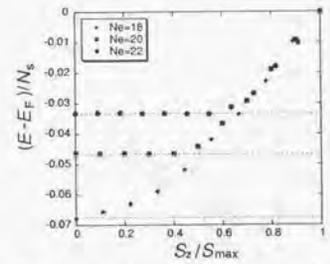

Figure 3.5: Energy per site as a function of the total S^z, measured from that of $S^z = S_{\rm max}$, for the t-ladder at $t = t_\perp = 1$ in a 16×2-site cluster with 22, 20 and 18 electrons starting from above. The solid and open symbols denote the data for $m = 50$ and $m = 100$, respectively.

state is a spin-singlet for $n = 0.5625$ and not for $n = 0.625$ and 0.6875. Hence, the phase boundary n_{c_2} is estimated as $n_{c_2} = 0.59 \pm 0.03$, which is consistent with Ref.[34]($n_{c_2} \simeq 0.6$). In this way, the phase boundary n_{c_2} is estimated for various $t_\perp/t$ as shown in Fig. 3.12. The region PF shrinks as $t_\perp/t$ increases, where PF is defined as the region which is neither FF nor SS. This is also consistent with the rigorous results in Sec. 3.2.

Here, we present the numerical results on the t-J ladder for small J and $J_\perp$. For simplicity, we choose $t_\perp = t$ and $J_\perp = J$, and set $t = 1$ as the energy unit. Figure 3.6 shows the n-dependence of $\Delta E_{\rm F}$ at $J = 0.00, 0.05, 0.07, 0.10$ and 0.15. As shown in this figure, $|\Delta E_{\rm F}|$ becomes large near half-filling ($n = 1$) due to antiferromagnetic correlation. Also, $|\Delta E_{\rm F}|$ seems to be the smallest near $n \simeq 0.8$ for $n > 0.5$. Figure 3.6 also indicates that $J = 0.05$ is enough to destroy the region FF.

Next, we consider the stability of PF against J. The ground-state energy as a function of the total S^z near half-filling for $J = 0.05, 0.07, 0.10$ and 0.15 is shown in Fig. 3.7. This figure suggests that FF is surrounded by PF in the phase diagram of the t-J ladder for

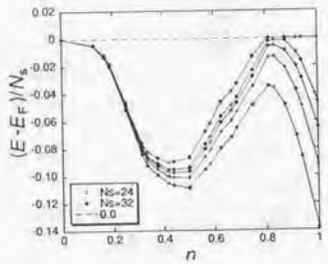

Figure 3.6: Energy difference ΔE_F per site as a function of filling for the t-J ladder in 12×2-site and 16×2-site clusters at $J/t = J_\perp/t = 0.00, 0.05, 0.07, 0.10$ and 0.15 starting from above. $t = t_\perp = 1$.

finite δ.

3.4 Metal-Insulator transition in the Hubbard ladder

In this section, we consider the metal-insulator (MI) transition at quarter-filling in the Hubbard ladder. In contrast to single chains[10, 39, 40] and planar models[41, 42, 43, 44, 45], there is a characteristic feature in ladder models, i.e. the band structure. The MI transition at quarter-filling is naturally understood, if one considers the weak-coupling limit ($U \to 0$) for large $t_\perp$. In the following subsection, we derive the effective Hamiltonian in this limit, by taking the band structure into account. (The MI transition in the two-dimensional Hubbard and t-J models will be discussed in Sec. 4.4.)

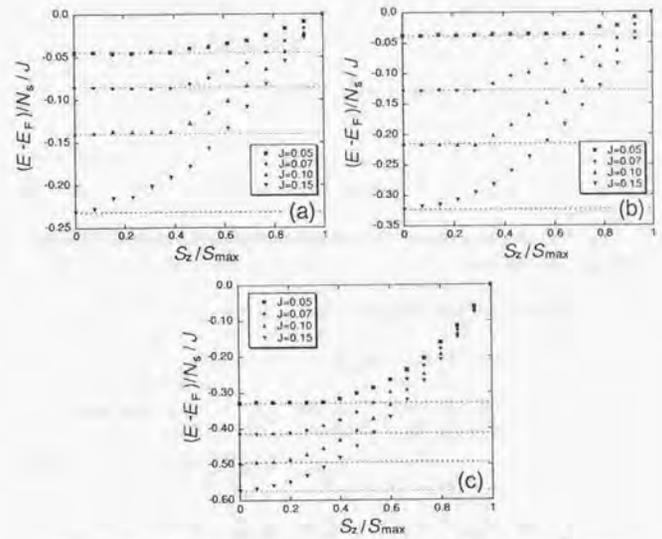

Figure 3.7: Energy per site as a function of the total S^z, measured from that of $S^z = S_{\max}$, for the t-J ladder at $t = t_\perp = 1$ in a 16×2-site cluster with 26 [(a)], 28 [(b)] and 30 [(c)] electrons at $J/t = J_\perp/t$ =0.05, 0.07, 0.10 and 0.15 starting from above. The dotted lines correspond to the energy of $S^z = 0$. The data are normalized by J.

3.4.1 MI transition at quarter-filling for $U << t_\perp$

Before discussing the MI transition for the $U = \infty$ Hubbard ladder at quarter-filling, let us consider the MI transition for $U << t_\perp$. The Hamiltonian of the Hubbard ladder is defined as

$$\begin{aligned}\mathcal{H} &= -t\sum_{i\sigma}(c^{1\dagger}_{i\sigma}c^{1}_{i+1\sigma} + c^{2\dagger}_{i\sigma}c^{2}_{i+1\sigma} + \text{h.c.}) \\ &\quad -t_\perp\sum_{i\sigma}(c^{1\dagger}_{i\sigma}c^{2}_{i\sigma} + \text{h.c.}) + U\sum_{i,\alpha} n^{\alpha}_{i\uparrow}n^{\alpha}_{i\downarrow},\end{aligned} \tag{3.7}$$

where $c^{\alpha\dagger}_{i\sigma}$ and $n^{\alpha}_{i\sigma}$ denote the creation operator and the number operator of an electron with spin σ at rung i in the α-th chain ($\alpha = 1, 2$), respectively.

This Hamiltonian can be rewritten in terms of bonding and anti-bonding operators as

$$\begin{aligned}\mathcal{H} &= -t\sum_{i\sigma}(b^{\dagger}_{i\sigma}b_{i+1\sigma} + a^{\dagger}_{i\sigma}a_{i+1\sigma} + \text{h.c.}) \\ &\quad -t_\perp\sum_{i\sigma}(n^{B}_{i\sigma} - n^{A}_{i\sigma}) \\ &\quad +\frac{U}{2}\sum_{i}(n^{B}_{i\uparrow} + n^{A}_{i\uparrow})(n^{B}_{i\downarrow} + n^{A}_{i\downarrow}) \\ &\quad +U\sum_{i}\{(b^{\dagger}_{i\uparrow}a_{i\downarrow} + a^{\dagger}_{i\uparrow}b_{i\downarrow})^2 + (b^{\dagger}_{i\downarrow}a_{i\downarrow} + a^{\dagger}_{i\downarrow}b_{i\downarrow})^2\},\end{aligned} \tag{3.8}$$

$$b^{\dagger}_{i\sigma} \equiv \frac{1}{\sqrt{2}}(c^{1\dagger}_{i\sigma} + c^{2\dagger}_{i\sigma}), \quad a^{\dagger}_{i\sigma} \equiv \frac{1}{\sqrt{2}}(c^{1\dagger}_{i\sigma} - c^{2\dagger}_{i\sigma}), \tag{3.9}$$

where $b^{\dagger}_{i\sigma}(a^{\dagger}_{i\sigma})$ and $n^{B}_{i\sigma}(n^{A}_{i\sigma})$ denote the creation operator and the number operator of an electron with spin σ at rung i in the (anti-)bonding band, respectively.

If $t_\perp$ is large enough, we can safely neglect contributions from the anti-bonding band, due to the second term in eq.(3.8). Thus, we obtain the effective Hamiltonian for the large inter-chain hopping ($t_\perp >> U$) as

$$\mathcal{H} = -t\sum_{i\sigma}(b^{\dagger}_{i\sigma}b_{i+1\sigma} + \text{h.c.}) + \frac{U}{2}\sum_{i} n^{B}_{i\uparrow}n^{B}_{i\downarrow}. \tag{3.10}$$

This is nothing but the Hubbard-chain Hamiltonian. Hence, it is naturally expected that the Mott transition occurs at quarter-filling for the Hubbard ladder, if the inter-chain hopping is large enough ($t_\perp >> U$).

3.4.2 Charge gap at quarter-filling for $U = \infty$

In this subsection, let us come back to the $U = \infty$ Hubbard ladder. Before discussing the metal-insulator transition, we consider the charge gap Δ_c at quarter-filling ($n = 0.5$). Figure 3.8 shows the n dependence of the chemical potential μ ($\equiv \partial E/\partial N_e$). The chemical potential μ in a finite-size cluster is defined as

$$\mu(\bar{n}) \equiv \frac{E(n_1) - E(n_2)}{(n_1 - n_2)N_s}, \tag{3.11}$$

where $E(n_i)$ denotes the ground-state energy at filling n_i, $i = 1, 2$, and $\bar{n} \equiv (n_1+n_2)/2$. We took $(n_2-n_1)N_s = 2$. The charge gap Δ_c is defined as $\Delta_c \equiv \mu(n_c+0) - \mu(n_c-0)$, where n_c is the critical electron-density ($n_c = 0.5$ in the present case). It is expected that the charge gap opens at quarter-filling, if $t_\perp/t$ is large enough (Sec. 3.2). Actually, for large values of $t_\perp/t$, the charge gap seems to open as shown in Fig. 3.8(a). For smaller values of $t_\perp/t$, we cannot determine whether the charge gap opens from Fig. 3.8. Thus, we extrapolate the charge gap in a finite-size cluster [eq.(3.12)] as $a + b/L$, using the data for $L = 12-24$, and estimate the charge gap as shown in Fig. 3.9.

$$\Delta_c(N_e = N_s/2) \equiv \frac{E(N_e = N_s/2+2) + E(N_e = N_s/2-2) - 2E(N_e = N_s/2)}{2}. \tag{3.12}$$

There are some possibilities for the critical value $t_{\perp c}/t$ above which the charge gap opens. One of the possibilities is that the critical value $t_{\perp c}/t$ is zero and that the gap is exponentially small for small $t_\perp/t$ as in the case of the Hubbard chain for small U/t[10]. In order to determine the critical value $t_{\perp c}/t$, we adopt the extended Aharonov-Bohm (AB) method proposed by Kusakabe and Aoki[46]. In the framework of this method, we investigate the extended spectral flow by introducing a Peierls phase as

$$\tilde{c}^{\alpha\dagger}_{i\sigma}\tilde{c}^{\alpha}_{i+1\sigma} \to \exp(i\frac{2\pi\Phi}{L\Phi_0})\tilde{c}^{\alpha\dagger}_{i\sigma}\tilde{c}^{\alpha}_{i+1\sigma}. \tag{3.13}$$

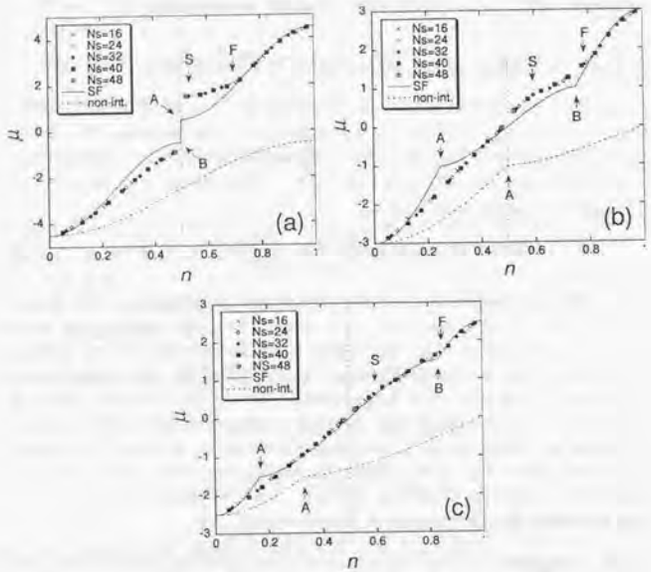

Figure 3.8: Chemical potential μ as a function of filling at $t_\perp/t$ =2.5 [(a)], 1.0 [(b)] and 0.5 [(c)]. For comparison, the chemical potential μ for the non-interacting case (dotted line) and that of the spinless fermion model (solid line) are shown ($N_s = 160 \times 2$). The points A and B correspond to the anomalies due to the band bottom of the anti-bonding band and the band top of the bonding band, respectively. The points F and S correspond to the phase boundaries n_{c_1} and n_{c_2}, respectively, which are estimated by the DMRG method (Sec. 3.3). $t = 1$.

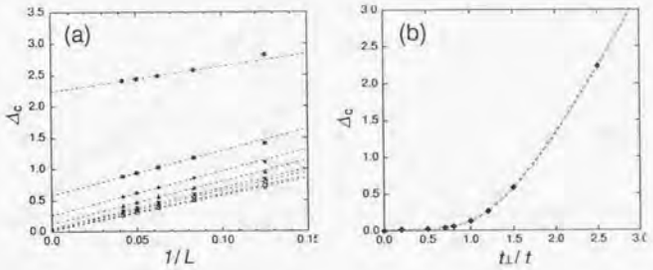

Figure 3.9: (a) Size dependence of the charge gap Δ_c for the t-ladder at $t_\perp/t$ =2.5, 1.5, 1.2, 1.0, 0.8, 0.7, 0.5 and 0.2 starting from above. (b) The charge gap Δ_c as a function of $t_\perp/t$. The bold line is a guide to the eye. $t = 1$.

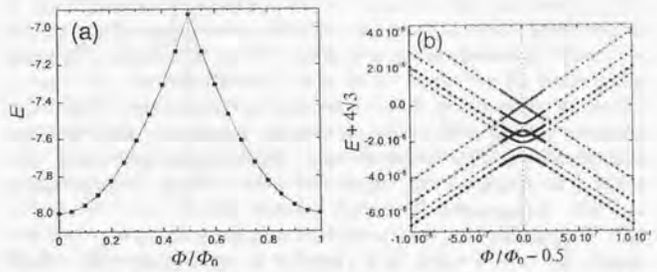

Figure 3.10: Spectral flow of the t-ladder for $t_\perp/t = 0.001$ in a 12-site cluster with 6 electrons for $0 \leq \Phi/\Phi_0 \leq 1$ [(a)], and the blow-up region for $\Phi/\Phi_0 \simeq 0.5$ [(b)]. The solid diamonds correspond to the spectral flow of the ground state. The data are obtained by the exact diagonalization method. $t = 1$.

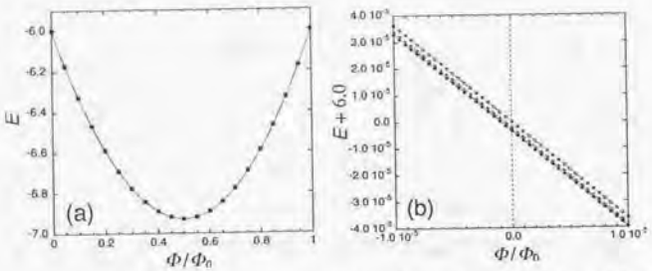

Figure 3.11: Spectral flow of the t-ladder for $t_\perp/t = 0.001$ in a 12-site cluster with 4 electrons for $0 \leq \Phi/\Phi_0 \leq 1$ [(a)], and the blow-up region for $\Phi/\Phi_0 \simeq 0$ [(b)]. The solid diamonds correspond to the spectral flow of the ground state. The data are obtained by the exact diagonalization method. $t = 1$.

It is expected that the period of the spectral flow reduces to $L\Phi_0/M$, if M-particle bound states are formed in the ground state. For example, $M = 1$ for a metallic state, and $M = 2$ for a BCS state. We apply this method to the t-ladder with a very small value of $t_\perp/t$ ($t_\perp/t = 0.001$). As shown in Fig. 3.10, the spectral flow at quarter-filling has the minimum extended AB period, i.e. $\Phi = \Phi_0$, suggesting that the ground state is an L-particle bound state or, in this case, an insulator[47]. This behavior is contrasted with the case off quarter-filling. For example, at $n = 1/3$, the extended AB period is larger than Φ_0 as shown in Fig. 3.11. This implies that the ground state at quarter-filling is an insulator already for $t_\perp/t = 0.001$. It is plausible to consider that the critical value $t_{\perp c}/t$ is probably zero. A possible scenario is the following: The perturbation of the small $t_\perp$-term produces a relevant Umklapp process which leads to an insulator, at the same time as the degeneracy with respect to the spin degrees of freedom is removed. The numerical results presented above are quite different from the case in the weak-coupling limit ($U \to +0$). In the weak-coupling limit, it is shown by bosonization that $t_{\perp c}/t$ is one[48]. Thus, it is expected that $t_{\perp c}/t$ decreases from 1

to 0 as the interaction U increases from 0 to ∞.

3.4.3 MI transition at quarter-filling for $U = \infty$

Now, let us consider the metal-insulator (MI) transition at quarter-filling. As discussed in Sec. 3.2, in the limit $t_\perp/t \to \infty$, the MI transition for $n \to 0.5 - 0$ is effectively described by the equivalent model to the $U \to \infty$ Hubbard chain, and the MI transition for $n \to 0.5 + 0$ is described by the spinless fermion model on a chain. It is interesting to compare these features with those in the weak-coupling regime. In the weak-coupling regime ($U \to +0$), the charge gap is also expected at quarter-filling for $t_\perp/t > 1$ because of the relevant Umklapp process[48]. This MI transition is understood as the Mott transition which is described by the $U \to +0$ Hubbard model on a chain written in terms of the bonding-band operators. On the other hand, for $U = \infty$, the low-energy effective Hamiltonian, in the large $t_\perp/t$ limit, is also the single-chain Hubbard Hamiltonian, where the inter-chain hopping $t_\perp$ of the ladder is regarded as the interaction U of the chain. Although in both weak-coupling [$U \ll t_\perp(> t)$] and strong-coupling [$U \gg t_\perp(\gg t)$] regimes, as $n \to 0.5 - 0$, the MI transition is described by single-chain effective Hubbard Hamiltonians, the value of the charge gap will have different energy scales. In the weak-coupling regime, the value of the charge gap would be determined mainly by U. On the other hand, in the strong-coupling regime, it would be determined mainly by $t_\perp$. This feature is similar to the two types of the MI transition for transition-metal compounds[49], i.e. the Mott-Hubbard type and the charge-transfer type.

3.5 Summary

In summary, two aspects of the ground state of the $U = \infty$ Hubbard ladder are investigated. One is ferromagnetism, the other is the metal-insulator (MI) transition. In the limit $t_\perp/t \to \infty$, it is rigorously shown, in a perturbative sense, that the ground state is a spin-singlet for $n \leq 0.5$ and that the total spin is maximum for $0.5 < n < 1$. For finite $t_\perp/t$, we have estimated the phase boundaries, with respect

to spontaneous magnetization, by the density-matrix renormalization group method. It is numerically shown that the region FF becomes larger and spreads down to quarter-filling as $t_\perp/t$ increases. This is consistent with the rigorous results presented in Sec. 3.2. The rigorous results ($t_\perp/t \to \infty$) and the numerical results for finite $t_\perp/t$ support one another and confirm that the ground state can be ferromagnetic for the $U = \infty$ Hubbard ladder with *finite hole-density*. The numerical results for the t-J ladder suggest that FF is surrounded by PF for finite δ in the small-J regime. We have also estimated the value of the charge gap at quarter-filling ($n = 0.5$). Applying the extended Aharonov-Bohm method, we have obtained numerical evidence that the critical value $t_{\perp c}/t$, above which the charge gap opens, is less than 0.001. This is quite different from that of the weak-coupling limit ($U \to +0$) ($t_{\perp c}/t = 1$)[48].

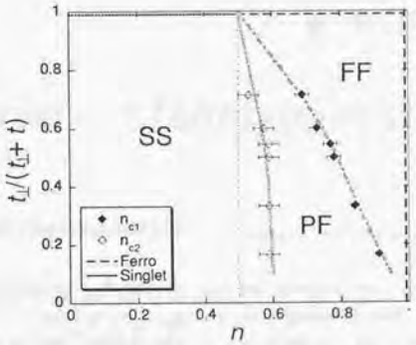

Figure 3.12: Phase diagram of the $U = \infty$ Hubbard ladder with respect to spontaneous magnetization. The dashed lines denote the region where the ground state is rigorously shown to have the maximum total spin S ($S = S_{\max}$) (Theorem 2 and Nagaoka's theorem). The dotted line in the limit $t_\perp/t \to \infty$ corresponds to the region where the ground state is shown to be a spin-singlet (Theorem 1). The solid and open diamonds correspond to the phase boundaries n_{c_1} and n_{c_2}, estimated by the DMRG method. The bold lines are guides to the eye. At $t_\perp/t = 0$, the ground states are degenerate with respect to the spin degrees of freedom, because the model reduces to the decoupled $U = \infty$ Hubbard chains. At quarter-filling, a charge gap is expected (Sec. 3.4).

Chapter 4

Two-dimensional t-J model

4.1 Introduction

In the previous chapter, we have investigated ground-state properties of the Hubbard ladder in the strong-coupling regime. A remarkable difference from the Hubbard chain in the strong-coupling regime is the existence of a ferromagnetic phase. As a next step, we would like to proceed to ground-state properties of the Hubbard-type models on a square lattice in the strong-coupling regime. Nagaoka's theorem also holds for the two-dimensional $U = \infty$ Hubbard model. Hence, there is a possibility that the ground state is ferromagnetic near half-filling in the large-U regime in two dimensions, too.

Also, in relation to the high-T_c superconductivity[5], a lot of attention has been given to the two-dimensional (2d) t-J model, because the 2d t-J model is considered as the simplest model that describes the low-energy properties of the copper-oxide planes[6, 22]. (See also Appendix A.1.) In order to understand the properties in the low-doping regime for high-T_c superconductors, the Mott transition in the Hubbard and t-J models has been studied[41, 42, 43, 44, 45, 50, 31, 51, 52, 53, 54, 55].

In this chapter, in order to see what happens in strongly-correlated electron systems in two dimensions, we review ground-state properties of the 2d t-J and Hubbard models reported so far. We focus our attention on ferromagnetism (Sec. 4.2), phase separation (Sec. 4.3) and the Mott transition (Sec. 4.4).

The t-J model is defined by the following Hamiltonian:

$$\mathcal{H}_{tJ} = -t \sum_{<i,j>\sigma} (\tilde{c}^{\dagger}_{i\sigma}\tilde{c}_{j\sigma} + \text{h.c.}) + J \sum_{<i,j>} (\boldsymbol{S}_i \cdot \boldsymbol{S}_j - \frac{1}{4} n_i n_j), \tag{4.1}$$

where $\tilde{c}^{\dagger}_{i\sigma}$ denotes a creation operator of an electron at site i with spin $\sigma(\sigma = \uparrow, \downarrow)$ with the constraint that no site is doubly occupied, which is defined as $\tilde{c}^{\dagger}_{i\sigma} \equiv (1 - n_{i-\sigma})c^{\dagger}_{i\sigma}$. The number operator $n_{i\sigma}$ is defined as $n_{i\sigma} \equiv c^{\dagger}_{i\sigma}c_{i\sigma}$, using the standard electron creation operator $c^{\dagger}_{i\sigma}$. The spin operator at site i is defined as $\boldsymbol{S}_i \equiv \frac{1}{2}\sum_{\alpha\beta} c^{\dagger}_{i\alpha}\boldsymbol{\sigma}_{\alpha\beta}c_{i\beta}$, where $\boldsymbol{\sigma}_{\alpha\beta}$ is the vector of Pauli matrices. The summation ($\sum_{<i,j>}$) is taken over all nearest neighbor sites on a square lattice.

4.2 Ferromagnetism

In this section, we briefly review itinerant ferromagnetism in the Hubbard and t-J models on a square lattice.

First, we would like to mention the results of the Hartree-Fock approximation for the 2d Hubbard model. In the framework of this approximation, fluctuations around the mean-field ($\bar{n}_\sigma \equiv \sum_i n_{i\sigma}/N_s$, N_s : the number of sites) are neglected. The condition for a ferromagnetic ground state is derived as

$$UN(\epsilon_F) > 1, \tag{4.2}$$

where U is the interaction strength of the Hubbard model, and $N(\epsilon_F)$ is the density of states at the Fermi level. This condition is known as the Stoner condition[56]. This condition probably captures some features of itinerant ferromagnetism. Large U and large $N(\epsilon_F)$ work for the enhancement of ferromagnetic correlations. For example, for $U = \infty$, Nagaoka's theorem ensures the existence of a ferromagnetic ground state, if the number of holes is one[7, 8, 9]. For $N(\epsilon_F) = \infty$, there are some models which are rigorously shown to have a ferromagnetic ground state[57, 58]. These models are called as flat-band models. However, it would also be true that the above approximation is naive and overestimates ferromagnetic correlations, because fluctuations around the mean-field are completely neglected. A problem is

how large these fluctuations modify the mean-field results. There is a possibility that quantum fluctuations are essentially important especially in low-dimensional systems in the strong-correlation regime. In the rest of this section, we review rigorous results and numerical results on itinerant ferromagnetism in the two-dimensional Hubbard and t-J models in the ground state.

4.2.1 $U = \infty$ Hubbard model

Let us consider the stability of Nagaoka's state for the $U = \infty$ Hubbard model. Nagaoka's theorem ensures that the ground state of the $U = \infty$ Hubbard model is a fully-polarized ferromagnetic state, if the number of holes (N_h) is one, under periodic boundary conditions. A question here is how stable Nagaoka's state is with hole doping.

- **Finite number of holes**
  As a first step, we consider the stability of the saturated ferromagnetic state for two-hole systems. It is possible to construct wavefunctions which have lower energy than the saturated ferromagnetic state for $N_h = 2$[59, 60, 61]. This means that the ground state of two-hole systems is not the saturated ferromagnetic state. However, this does not mean that ferromagnetism cannot be realized in the thermodynamic with finite hole density, because the hole density $\delta \equiv N_h/N_s$ goes to zero, as the number of sites N_s approaches infinity with N_h fixed.

  Actually, it is shown that, for any finite number of holes, the ground states in finite-size clusters become asymptotically degenerate with the saturated ferromagnetic state as $N_s \to \infty$[62, 63, 64, 65].

- **Finite hole density : variational bounds**
  Next, we consider the stability of the saturated ferromagnetic state with finite hole doping. Hereafter, δ_c denotes the critical hole density, above which the ground state is not the saturated ferromagnetic state. This δ_c is estimated by various approaches.

  One approach is to construct wavefunctions which have lower energy than the saturated ferromagnetic state. This approach provides the upper bound of δ_c. Shastry, *et.al.* obtained the upper bound as $\delta_c < 0.49$ for the square lattice[66]. Basile and Elser improved the upper bound as $\delta_c < 0.41$[67]. Furthermore, von der Linden and Edwards improved it as $\delta_c < 0.29$[68], and Wurth, *et.al.* obtained $\delta_c < 0.251$[69]. As far as we know, the upper bound was reduced to $\delta_c < 0.237$[70].

- **Finite hole density : exact diagonalization**
  Another approach is to calculate δ_c numerically in finite-size clusters and extrapolate it to the thermodynamic limit. However, it is difficult to obtain reliable results for large-size systems by numerical calculations for finite hole density. In small-size systems, the total spin of the ground state depends strongly on the boundary conditions.

  Takahashi investigated the total spin of the ground state in various types of clusters by exact diagonalization[26]. From his numerical data, he deduced the following tendency for bipartite lattices: There is not a strongly ferromagnetic region except for Nagaoka's case. The ground state is paramagnetic or at most weakly ferromagnetic in many cases.

  Riera and Young investigated the ground-state total spin in a larger (16-site) cluster by exact diagonalization[28]. They also found non-monotonic behavior of the total spin as a function of N_h, if boundary conditions are fixed. They took an average of the total spins in the following cases: One is under periodic boundary conditions for both directions, and the other is under the periodic boundary condition in one direction and the anti-periodic boundary condition in the other. They obtained fairly monotonic behavior as a function of N_h. Furthermore, they found that the total spin per N_e never decreases as the size increases, where N_e is the number of electrons. From these results, they inferred that the ground state of the $U = \infty$ Hubbard model in 2d is probably ferromagnetic for finite δ near half-filling. However, they did not answer the question whether this ferromagnetic state is the saturated ferromagnetic state or a partially-polarized ferromagnetic state.

Liang and Pang applied the density-matrix renormalization group (DMRG) method to this problem[34]. This method is quite efficient for quasi-one dimensional systems[35]. They investigated the multi-leg ladders for $N_l = 2 - 4$, where N_l denotes the number of legs. Within the numerical accuracy, they found little N_l dependence of δ_c. Hence, they concluded that δ_c is about 0.22 in two dimensions, and that the total spin gradually decreases as δ increases. The ground state becomes paramagnetic for $\delta_c \gtrsim 0.4$.

- **Finite hole density : high-temperature expansion**
  Another approach to determine δ_c is to extrapolate high-temperature results to the low-temperature regime.

  Yedidia applied the high-temperature expansion technique to this model, and found a ferromagnetic region as $\delta < 3/11$, where the susceptibility diverges as $\chi(q=0) \propto T^{\gamma}$ $(\gamma > 1)$[29].

  Putikka, *et.al.* also used the high-temperature expansion technique to estimate δ_c[32]. One of their results is that the ground-state energy of the $U = \infty$ Hubbard model is always lower than that of Nagaoka's state except for the low-doping limit. This implies that there is no region of Nagaoka's state for finite hole density, i.e. $\delta_c = 0$. They used the criterion of Yedidia and found the region, where the susceptibility diverges as $\chi(q=0) \propto T^{\gamma}$ $(\gamma > 1)$, for $\delta \lesssim 0.3$. They interpreted this region as that of a ferrimagnetic state (i.e. a partially-polarized ferromagnetic state).

- **Finite hole density : quantum Monte Carlo**
  Zhang, *et.al.* applied a quantum Monte Carlo method to ferromagnetism in the $U = \infty$ Hubbard model[30]. They calculated magnetization at inverse temperature $\beta t = 2$ in a small magnetic field. Their numerical data suggest exponential decay of magnetization with doping.

4.2.2 t-J model

Now, let us consider the stability of ferromagnetism against J for the t-J model and finite U for the Hubbard model.

- **Hubbard model : variational bounds of Nagaoka's state**
  For the Hubbard model, the stability of the saturated ferromagnetic state is investigated by variational approaches. Hereafter, U_{cr} denotes the maximum value of U below which Nagaoka's state is unstable for all hole densities. The lower bound of U_{cr} is estimated, if one finds a wavefunction which has lower energy than Nagaoka's state for finite U. In the paper by von der Linden and Edwards, they estimated the lower bound of U_{cr} as $U_{cr} > 42t$[68]. Hanisch, *et.al.* obtained it as $U_{cr} > 63.62t$[71]. As far as we know, the lower bound of U_{cr} was raised to $U_{cr} > 77.7t$[69].

- **t-J model : numerical study**
  Putikka, *et.al.* applied the high-temperature expansion technique to the 2d t-J model[31, 32]. According to their numerical results and their criterion, Nagaoka's state is unstable for both hole doping and the antiferromagnetic interaction (J-term in the t-J model). However, they found the region, where the susceptibility diverges as $\chi(q=0) \propto T^{\gamma}$ $(\gamma > 1)$, for finite J. They interpreted this region as ferrimagnetic. Their calculation suggests that this ferrimagnetic phase survives for $J \lesssim 0.1$.

  The stability of Nagaoka's state in the t-J model is investigated by exact diagonalization. Kusakabe and Aoki fitted the crossover points J_c between Nagaoka's state (the spiral state) and the antiferromagnetic state for one hole (two holes) in the form $J_c \propto \delta^{\alpha}$. They estimated $\alpha = 1.73$ for one hole, and $\alpha = 1.74$ for two holes. This implies that the critical value of J_c approaches zero as the system-size increases with N_h fixed. Thus, the ferromagnetic state is unstable with the antiferromagnetic interaction (J-term) in the low-doping limit.

4.3 Phase separeation

In this section, we consider phase separation in the 2d t-J model. It is naturally expected that if the exchange coupling J is large enough, phase separation occurs in the ground state of the t-J model. Hereafter, the value of J, above which phase separation occurs at electron density

Table 4.1: Estimation of $J_c(n \to 1)$

Author(s)	$J_c(n \to 1)$	Method	Ref.
Emery, *et.al.*	$J_c \simeq 0$	Lanczos (16 sites)	Ref.50, 1990
Putikka, *et.al.*	$J_c \simeq 1.2$	High-temp. expansion	Ref.31, 1992
Dagotto, *et.al.*	$J_c \simeq 1$	Lanczos (16 sites)	Ref.51, 1992
Prelovšek, *et.al.*	$J_c \simeq 1.5$	Lanczos (20 sites)	Ref.52, 1993
Poilblanc	$J_c \simeq 0.75$	Lanczos (26 sites)	Ref.53, 1995
Kohno	$J_c \simeq 0.75$	Power Lanczos	Ref.45, 1997
Hellberg, *et.al.*	$J_c \simeq 0$	Power method	Ref.54, 1997
Shih, *et.al.*	$J_c \simeq 0.6$	Power Lanczos	Ref.55, 1997

n, is denoted by $J_c(n)$. For one dimension, the phase-separation boundary is estimated by exact diagonalization[72]. For two dimensions, there are some numerical studies on the phase-separation boundary. In the limit of the low electron density, the phase-separation boundary is obtained very accurately as $J_c(n \to 0) = 3.4367 \pm 0.0001$ by solving the equation of motion of the two-electron system[73]. In the intermediate region of the electron density, the phase boundary has a negative slope ($\mathrm{d}J_c/\mathrm{d}n < 0$)[50], in contrast to the one-dimensional case[72]. Near half-filling, the results on the boundary $J_c(n \to 1)$ are controversial. Some groups insist that phase separation occurs at all J, others claim that there is a finite region of J where phase separation does not occur. Numerical results reported so far are summarized in table 4.1.

- **Phase separation at all J**
  Emery, *et.al.* investigated phase separation in the 2d t-J model by exact diagonalization[50]. They analyzed their numerical data in a 16-site cluster based on the Maxwell construction. They interpreted the non-monotonic behavior of the chemical potential with doping as an indication of phase separation. They concluded that phase separation occurs for any value of J/t in two dimensions.

  Hellberg and Manousakis investigated phase separation in the 2d t-J model by a projector Monte Carlo method called as the power method[54]. They calculated the ground-state energy, and analyzed it based on the Maxwell construction. They also concluded that phase separation occurs for any J.

- **Finite $J_c(n \to 1)$**
  Putikka, *et.al.* applied the high-temperature expansion technique to this problem[31]. They estimated the phase-separation boundary from the behavior of the charge susceptibility. Their numerical results suggest that phase separation does not occur for $J/t \lesssim 1.2$.

  Dagotto, *et.al.* also investigated phase separation in the 2d t-J model by exact diagonalization[51]. They concluded that there is a finite region of J, where phase separation does not occur. They interpreted the region, where Emery, *et.al.* considered that phase separation occurs for small J, as the region where bound states are formed.

  Prelovšek and Zotos calculated the two-point and four-point density correlations for four-hole systems by exact diagonalization[52]. They obtained indications of an instability toward an inhomogeneous hole distribution for $J/t \gtrsim 1.5$.

  Furthermore, Poilblanc investigated the ground-state properties of the 2d t-J model in the low-doping regime by exact diagonalization in clusters up to 26 sites[53]. He obtained results that support the existence of homogeneous states in the small J regime near half-filling.

  The present author investigated the ground-state properties of the 2d t-J model by a projector Monte Carlo method called as the power Lanczos method[74] and by exact diagonalization[45]. He analyzed the numerical data based on the Maxwell construction, and hyperscaling hypothesis. His numerical results suggest that the Mott transition is a second-order transition for $J/t \simeq 0.5$.

  Recently, Shih, *et.al.* reexamined the phase-separation boundary by the power Lanczos method[55]. They also concluded that there is a finite region of J, where phase separation does not occur ($J/t \lesssim 0.6$).

- **Experimental indication**
  NQR measurements for $La_{2-x}Sr_xCuO_4$ ($x = 0.02 - 0.08$) indicate that mesoscopic domains with local antiferromagnetic order are formed rather than a conventional spin-glass state in the low-doping regime[75].

4.4 Mott transition

In the previous section, we have seen indications of phase separation in the 2d t-J model. In the parameter regime where phase separation occurs, the Mott transition is of first order. In this section, we review studies on the second-order Mott transition.

Scaling theory is useful not only to classify critical phenomena, but also as a guide to analyze numerical and experimental data. Fisher, *et.al.* discussed the superfluid-insulator transition in the dirty and pure Bose-Hubbard models on the basis of hyperscaling theory[76]. Imada extended their argument to the metal-insulator transition, and analyzed numerical results of the two-dimensional (2d) Hubbard model[43]. In this section, we briefly review numerical results on the Mott transition in the 2d Hubbard and t-J models and its analysis based on hyperscaling theory. The derivation of the scaling relations is shown in Appendix A.3[43].

- **Hyperscaling theory**
  According to hyperscaling theory, a single length scale ξ, which is related to the Mott transition, diverges as

$$\xi \propto \delta^{-1/d}, \tag{4.3}$$

  where d and δ denote the spatial dimensionality and the doping concentration, respectively. Also, the charge susceptibility behaves as

$$\chi_c \propto \delta^{1-z/d}, \tag{4.4}$$

  where z is the dynamical exponent, which relates the length scale ξ to the energy scale Ω as $\Omega \propto \xi^{-z}$. Here, χ_c is the charge susceptibility defined as the derivative of the electron density n with

respect to the chemical potential μ, i.e. $\chi_c \equiv \partial n/\partial\mu$. Hyperscaling theory also predicts that

$$\xi \propto \Delta^{-1/z}, \tag{4.5}$$

  where Δ is a control parameter which measures the distance from the critical point. For the generic transition controlled by the filling, the chemical potential shift $|\mu - \mu_c|$ corresponds to Δ.

- **Metal-insulator transition : Hubbard model**
  Now, let us see the critical behavior of the Mott transition in the 2d Hubbard model. Furukawa and Imada investigated the Mott transition of the 2d Hubbard model in the ground state by a quantum Monte Carlo method[41]. They took $U = 4$. They obtained numerical results showing that the peak value of the spin structure factor $S_{\max}(Q)$ diverges as

$$S_{\max}(Q) \propto \delta^{-1}. \tag{4.6}$$

  They assumed that the spin-spin correlation behaves as $\langle \boldsymbol{S}_o \cdot \boldsymbol{S}_r \rangle \propto e^{iQr} \cdot e^{-r/\xi_m}$. Under this assumption, eq.(4.6) implies that the antiferromagnetic correlation length ξ_m, diverges as

$$\xi_m \propto \delta^{-1}. \tag{4.7}$$

  This behavior is consistent with eq.(4.3) obtained by the scaling theory. They also investigated the doping dependence of the chemical potential μ. Their numerical data can be fitted well as

$$|\mu - \mu_c| \propto \delta^2. \tag{4.8}$$

  This implies that the charge susceptibility χ_c diverges as

$$\chi_c \propto \delta^{-1}. \tag{4.9}$$

  According to eq.(4.4), the dynamical exponent z is obtained as $z = 4$.

- **Insulator-metal transition : Hubbard model**
  Assaad and Imada investigated the insulator-metal transition in

the 2d Hubbard model at $U = 4$[44]. They calculated the localization length ξ_l defined as $G(\vec{r}, \omega = \mu) \sim e^{-|\vec{r}/\xi_l|}$ at half-filling, where $G(\vec{r}, \omega = \mu)$ is the single-particle Green function with distance $|\vec{r}|$ and chemical potential μ. They obtained numerical results suggesting that

$$\xi_l \propto |\mu - \mu_c|^{-1/4}. \tag{4.10}$$

This behavior implies that z is four, due to eq.(4.5). The numerical results for the 2d Hubbard model at $U = 4$ support the scaling hypothesis, and suggest that the Mott transition in the 2d Hubbard model is characterized by $z = 4$. This behavior is contrasted with the non-interacting fermion systems on a lattice. In this case, the dynamical exponent z is two.

- **Mott transition : t-J model**
  The present author investigated the doping dependence of the chemical potential and the peak value of the spin structure factor for the 2d t-J model at $J/t = 0.5$[45]. He assumed that the transition is of second order, and analyzed numerical results based on hyperscaling theory. He obtained qualitatively the same results as those of the 2d Hubbard model at $U = 4$. His numerical results suggest that the Mott transition is characterized by $z = 4$ for the 2d t-J model in the small-J regime.

- **Experiments**
  Now, let us see experimental features for high-T_c cuprates.

  As for the spin degrees of freedom, neutron scattering experiments suggest that the doping dependence of the antiferromagnetic correlation length ξ_m behaves as $\xi_m \propto \delta^{-1/2}$[77]. This is consistent with hyperscaling theory and numerical results.

  For the charge degrees of freedom, divergent behavior of the charge susceptibility was recently observed by a photo-emission experiment[78].

4.5 Summary

In summary, ferromagnetism and the Mott transition in the two-dimensional t-J and Hubbard models have been reviewed. Owing to the progress of computational techniques, a lot of indications have been obtained. Most of the numerical studies on ferromagnetism suggest the existence of a kind of ferromagnetic state in the low-doping regime. Also, it is suggested numerically that phase separation occurs in a large parameter regime for the 2d t-J model. However, following issues have not been settled yet: (i) whether the Mott transition in the 2d t-J model is a first-order or second-order transition in the realistic parameter regime ($J/t \simeq 0.5$) for high-T_c superconductors, and (ii) whether the ground state can really be ferromagnetic with finite hole-density. (iii) Furthermore, the relation between the ground state of the t-J model and that of the Hubbard model has not been clarified yet.

In part II, we consider the attractive Hubbard model with nearest neighbor repulsion as the simplest case where a superconductor-insulator transition occurs.

Part II

Attractive Hubbard model

Chapter 5

$U \to -\infty$ extended Hubbard model

5.1 Effective model up to order $t^2/|U|$

In this subsection, we derive the effective Hamiltonian $\mathcal{H}^{\rm eff}$ of the negative U Hubbard model with nearest neighbor repulsion in the large-$|U|$ limit, up to order $t^2/|U|$[79, 80].

We consider the extended attractive (ext$-U$) Hubbard model defined as

$$\begin{aligned}\mathcal{H}_{\rm ext-U} &\equiv -t\sum_{\langle i,j\rangle\sigma}(c_{i\sigma}^\dagger c_{j\sigma}+{\rm h.c.})-|U|\sum_i(n_{i\uparrow}-1/2)(n_{i\downarrow}-1/2)\\ &\quad +V\sum_{\langle i,j\rangle}(n_i-1)(n_j-1)-\mu\sum_i n_i,\end{aligned}\tag{5.1}$$

where $\langle i,j\rangle$ denotes nearest neighbors. Here, n_i is the number operator at site i. For $V=0$, the attractive Hubbard model is recovered. Transforming the ext$-U$ Hubbard model by

$$\begin{cases} c_{i\uparrow} \to a_{i\uparrow}, \\ c_{i\downarrow} \to a_{i\downarrow}^\dagger, \end{cases}$$

we obtain the anisotropic repulsive (anis$+U$) Hubbard model:

$$\mathcal{H}_{\rm anis+U} = \mathcal{H}_{zt}+\mathcal{H}_{zU}+\mathcal{H}_{zJ}+\mathcal{H}_{zH}+\mathcal{H}_{z\rm const},\tag{5.2}$$

$$\begin{aligned}\mathcal{H}_{zt} &\equiv -t\sum_{\langle i,j\rangle\sigma}(\sigma a_{i\sigma}^\dagger a_{j\sigma}+{\rm h.c.}),\\ \mathcal{H}_{zU} &\equiv |U|\sum_i(n_{i\uparrow}^a-1/2)(n_{i\downarrow}^a-1/2),\quad n_{i\sigma}^a\equiv a_{i\sigma}^\dagger a_{i\sigma},\\ \mathcal{H}_{zJ} &\equiv J^z\sum_{\langle i,j\rangle}S_i^{az}S_j^{az},\quad J^z\equiv 4V,\quad S_i^{az}\equiv\frac{1}{2}(n_{i\uparrow}^a-n_{i\downarrow}^a),\\ \mathcal{H}_{zH} &\equiv -H^a\sum_i S^{az},\quad H^a\equiv 2\mu,\\ \mathcal{H}_{z\rm const} &\equiv -N_s\Delta E,\quad \Delta E\equiv\mu,\end{aligned}$$

where N_s denotes the number of sites. For bipartite lattices, by gauge transformation $a_{i\downarrow}\to(-1)^i a_{i\downarrow}$, we can transform $\mathcal{H}_{zt}$ to

$$\mathcal{H}'_{zt}=-t\sum_{\langle i,j\rangle\sigma}(a_{i\sigma}^\dagger a_{j\sigma}+{\rm h.c.}).\tag{5.3}$$

Without the external magnetic field H for the ext$-U$ Hubbard model, the filling n^a for the anis$+U$ Hubbard model is 1/2, i.e. half-filled. Hence, in the limit $|U|\to\infty$, the anis$+U$ Hubbard model reduces to the spin-1/2 XXZ model:[1]

$$\begin{aligned}\mathcal{H}_{XXZ} &= J\sum_{\langle i,j\rangle}\{\boldsymbol{S}_i^a\boldsymbol{S}_j^a+(\lambda-1)S_i^{az}S_j^{az}\},\\ &\quad J=4t^2/|U|,\quad \lambda=J^z/J+1,\end{aligned}\tag{5.4}$$

where $\boldsymbol{S}_i^a$ denotes the spin operator at site i defined as $\boldsymbol{S}_i^a\equiv\frac{1}{2}\sum_{\alpha\beta}a_{i\alpha}^\dagger\boldsymbol{\sigma}_{\alpha\beta}a_{i\beta}$. Here, $\boldsymbol{\sigma}$ denotes the vector of Pauli matrices. The chemical potential μ of the ext$-U$ Hubbard model corresponds to the external field H^a of the XXZ model. As a result, the doping dependence for the ext$-U$ Hubbard model, in the limit $|U|\to\infty$, corresponds to the magnetization process of the spin-1/2 XXZ model. For $V=0$, the XXZ model reduces to the XXX (SU(2) Heisenberg) model.

5.2 Spin-1/2 XXZ chain

As a first step, in this section, we review the Bethe ansatz results for the magnetization process of the spin-1/2 XXZ chain[14].

[1] Here, we neglect constant terms.

The spin-1/2 XXZ chain is defined by the following Hamiltonian:

$$\mathcal{H} \equiv J\sum_i (S_i^x S_{i+1}^x + S_i^y S_{i+1}^y + \lambda S_i^z S_{i+1}^z), \tag{5.5}$$

where $S_i^{x(y,z)}$ denote the $x(y,z)$ components of the spin operator at site i. The anisotropic coupling constant is denoted by λ. For $\lambda = 1$, the isotropic Heisenberg model is recovered. Hereafter, we assume the periodic boundary condition, i.e. $S_{L+1}^{x(y,z)} = S_1^{x(y,z)}$, where L denotes the length of a chain.

Let $f(x_1, \cdots, x_{N_1})$ be the amplitude in the wavefunction when down spins are located at sites $x_1, \cdots, x_{N_1}$ $(x_1 < x_2 < \cdots < x_{N_1})$, where N_1 denotes the number of down spins. The amplitude f is expressed under the Bethe ansatz as

$$f(x_1, \cdots, x_{N_1}) = \sum_P \exp(\mathrm{i}\sum_{j=1}^{N_1} k_{P_j} x_j + \frac{\mathrm{i}}{2}\sum_{j<l} \phi_{P_j P_l}), \tag{5.6}$$

where $P = (P1, P2, \cdots, PN_1)$ is a permutation of $(1, 2, \cdots, N_1)$, and $\phi_{ij} = -\phi_{ji}$. The quasi-momenta k_i's and phases ϕ_{ij}'s are determined to satisfy the Schrödinger equation with the periodic boundary condition. If the following relations are satisfied, we obtain eigenfunctions with energy $E = J\sum_{j=1}^{N_1}(\cos k_j - \lambda) + \frac{J\lambda L}{4}$.

$$\cot\frac{\phi_{jl}}{2} = \lambda \sin(\frac{k_j - k_l}{2})/\{\cos(\frac{k_j + k_l}{2}) - \lambda\cos(\frac{k_j - k_l}{2})\}, \tag{5.7}$$

and due to the periodic boundary condition,

$$Lk_j = 2\pi I_j^0 + \sum_{l=1}^{N_1} \phi_{jl}. \tag{5.8}$$

where I_j^0 is an integer. Equations (5.7) and (5.8) lead to

$$L(k_j - \pi) = 2\pi I_j - 2\sum_{l=1}^{N_1} \tan^{-1}[\lambda \sin(\frac{k_j - k_l}{2})/\{\cos(\frac{k_j + k_l}{2}) - \lambda\cos(\frac{k_j - k_l}{2})\}], \tag{5.9}$$

where $I_j \equiv (2I_j^0 - L + N_1 - 1)/2$. For even L, I_j is an integer (a half-odd integer), if N_1 is odd (even).

For the ground state, $I_j = (\frac{N_1-1}{2}, \frac{N_1-3}{2}, \cdots, -\frac{N_1-1}{2},)$. Especially for the XY chain $(\lambda = 0)$, $k_j = \pi + \frac{2\pi I_j}{L}$.

Let us consider the magnetization process of the spin-1/2 XXZ chain. For $\lambda \leq 1$, the low-lying excitation is gapless. For $\lambda > 1$, an excitation gap opens. In the rest of this section, we derive the explicit form of the excitation gap and the magnetization curve in the limit $m \to +0$ for $\lambda > 1$, where m denotes the magnetization per site.

For $\lambda > 1$, we introduce ϕ_i defined as

$$\cot\frac{k_i}{2} = \coth\frac{\Phi}{2}\tan\frac{\phi_i}{2}, \tag{5.10}$$

where Φ is defined by

$$\cosh\Phi \equiv \lambda. \tag{5.11}$$

In terms of ϕ_i's, eq.(5.7) is rewritten as

$$\cot\frac{\phi_{jl}}{2} = \coth\Phi\tan(\frac{\phi_j}{2} - \frac{\phi_l}{2}). \tag{5.12}$$

Thus, eq.(5.9) is rewritten as

$$L\{2\tan^{-1}(\tanh\frac{\Phi}{2}\cot\frac{\phi_j}{2}) - \pi\} = 2\pi I_j - 2\sum_{l=1}^{N_1}\tan^{-1}[\coth\Phi\tan(\frac{\phi_j}{2} - \frac{\phi_l}{2})], \tag{5.13}$$

In the thermodynamic limit, eq.(5.13) becomes

$$2\tan^{-1}(\tanh\frac{\Phi}{2}\cot\frac{\phi}{2}) - \pi = 2\pi g(\phi) - 2\int_{-Q}^{Q}\tan^{-1}[\coth\Phi\tan(\frac{\phi}{2} - \frac{\phi'}{2})]\rho(\phi')\mathrm{d}\phi', \tag{5.14}$$

where

$$g(\phi) = \lim_{L, N_1 \to \infty}\frac{I_j}{L}, \quad \rho(\phi) = \frac{\mathrm{d}g(\phi)}{\mathrm{d}\phi}. \tag{5.15}$$

Taking the derivative with respect to ϕ, we obtain

$$\rho(\phi) + \int_{-Q}^{Q}\frac{1}{2\pi}\frac{\sinh 2\Phi}{\cosh 2\Phi - \cos(\phi - \phi')}\rho(\phi')\mathrm{d}\phi' = \frac{1}{2\pi}\frac{\sinh\Phi}{\cosh\Phi - \cos\phi}. \tag{5.16}$$

The magnetization density $m(\equiv \lim_{L\to\infty} S^z/L)$ and the energy density $e(\equiv \lim_{L\to\infty} E/L)$ are obtained as

$$m = \frac{1}{2} - \int_{-Q}^{Q} \rho(\phi)\mathrm{d}\phi, \tag{5.17}$$

$$e = -J\int_{-Q}^{Q} \frac{\sinh^2\Phi}{\cosh\Phi - \cos\phi}\rho(\phi)\mathrm{d}\phi + \frac{J\lambda}{4}, \tag{5.18}$$

where $0 \le Q \le \pi$.

For the ground state ($Q = \pi$), we can solve eq.(5.16) by the Fourier transformation, and obtain

$$\rho_0(\phi) = \frac{1}{4\pi}\sum_{n=-\infty}^{\infty} \frac{\mathrm{e}^{\mathrm{i}n\phi}}{\cosh n\Phi}. \tag{5.19}$$

Using this $\rho_0(\phi)$, we obtain the magnetization density and the energy density in the ground state as

$$m_0 = 0, \quad e_0 = -J\sinh\Phi\cdot[\frac{1}{2} + 2\sum_{n=1}^{\infty}\frac{1}{1+\mathrm{e}^{2n\Phi}}] + \frac{J\lambda}{4}. \tag{5.20}$$

Now let us consider the deviation from the ground state. We put $Q = \pi - \epsilon$ and expand $\rho(\phi)$, m and e with respect to ϵ, assuming that ϵ is small. The solution of eq.(5.16) with $Q = \pi - \epsilon$ for small ϵ is expanded as

$$\begin{aligned}
\rho(\phi) &= \rho_0(\phi) + \epsilon\rho_1(\phi) + \epsilon^2\rho_2(\phi) + \epsilon^3\rho_3(\phi) + \cdots, \\
\rho_1(\phi) &= \frac{1}{2\pi}\sum_{n=-\infty}^{\infty}\frac{2(-1)^n\rho_0(\pi)\mathrm{e}^{\mathrm{i}n\phi}}{1+\mathrm{e}^{|2n\phi|}}, \\
\rho_2(\phi) &= \frac{1}{2\pi}\sum_{n=-\infty}^{\infty}\frac{2(-1)^n\rho_1(\pi)\mathrm{e}^{\mathrm{i}n\phi}}{1+\mathrm{e}^{|2n\phi|}}, \\
\rho_3(\phi) &= \frac{1}{2\pi}\sum_{n=-\infty}^{\infty}\frac{(-1)^n(6\rho_2(\pi)+\rho_0''(\pi)-n^2\rho_0(\pi))\mathrm{e}^{\mathrm{i}n\phi}}{3(1+\mathrm{e}^{|2n\phi|})},
\end{aligned} \tag{5.21}$$

where $\rho_i'(\phi)$ denotes the derivative of $\rho_i(\phi)$ with respect to ϕ, and

$$\begin{aligned}
\rho_0(\pi) &= \frac{1}{4\pi}\sum_{n=-\infty}^{\infty}\frac{(-1)^n}{\cosh n\Phi}, \quad \rho_1(\pi) = \frac{1}{\pi}\sum_{n=-\infty}^{\infty}\frac{\rho_0(\pi)}{1+\mathrm{e}^{|2n\phi|}}, \\
\rho_2(\pi) &= \frac{1}{\pi}\sum_{n=-\infty}^{\infty}\frac{\rho_1(\pi)}{1+\mathrm{e}^{|2n\phi|}}, \quad \rho_0''(\pi) = -\frac{1}{4\pi}\sum_{n=-\infty}^{\infty}\frac{n^2(-1)^n}{\cosh n\Phi}.
\end{aligned}$$

The magnetization density is also expanded as

$$\begin{aligned}
m &= m_0 + \epsilon m_1 + \epsilon^2 m_2 + \epsilon^3 m_3 + \cdots, \\
m_1 &= \rho_0(\pi), \quad m_2 = \rho_1(\pi), \quad m_3 = \rho_2(\pi) + \frac{\rho_0''(\pi)}{6}.
\end{aligned} \tag{5.22}$$

The energy density is expanded as

$$\begin{aligned}
e &= e_0 + \epsilon e_1 + \epsilon^2 e_2 + \epsilon^3 e_3 + \cdots, \\
e_1 &= 4\pi J\sinh\Phi\cdot\rho_0(\pi)^2, \quad e_2 = 4\pi J\sinh\Phi\cdot\rho_0(\pi)\rho_1(\pi), \\
e_3 &= 4\pi J\sinh\Phi\cdot\rho_0(\pi)\{\rho_2(\pi) + \frac{\rho_0''(\pi)}{3}\}.
\end{aligned} \tag{5.23}$$

Hence, e is expanded with respect to m for small m as

$$e = e_0 + 4\pi J\sinh\Phi\cdot\rho_0(\pi)\{m + \frac{\rho_0''(\pi)}{6\rho_0(\pi)^3}m^3\} + O(m^4). \tag{5.24}$$

The magnetic field H in the limit $m \to +0$ is obtained as

$$H_c = \frac{\partial e}{\partial m}|_{m\to+0} = 4\pi J\sinh\Phi\cdot\rho_0(\pi). \tag{5.25}$$

This H_c corresponds to the critical field above which the ground state has nonzero magnetization, and also to the energy gap $\Delta_g \equiv E(S^z = 1) - E(S^z = 0)$. Near the isotropic point ($\lambda \gtrsim 1$), H_c is exponentially small[81] as

$$H_c \simeq 4\pi J\exp[-\frac{\pi^2}{2\sqrt{2(\lambda-1)}}]. \tag{5.26}$$

From eq.(5.24), it is shown that the magnetization curve in the limit $m \to +0$ has an infinite slope as

$$m \propto \sqrt{H - H_c}. \tag{5.27}$$

It should be noted that the spin-1/2 XXZ chain exhibits a second order transition with respect to the magnetic field in the ground state.

Chapter 6

Spin-1/2 XXZ models

6.1 Introduction

In Sec. 5.2, we have seen that the spin-1/2 XXZ chain with Ising-like anisotropy exhibits a second-order transition in a magnetic field. This phase transition corresponds to the metal-insulator transition at half-filling in the $U \to -\infty$ Hubbard chain with nearest neighbor repulsion. According to hyperscaling theory introduced in chapter 4, this metal-insulator transition is classified into the universality class of the dynamical exponent $z = 2$. For one dimension, in many cases, metal-insulator transitions belong to this universality class. As seen in chapter 4, in two-dimensional interacting fermion systems such as the 2d Hubbard model, the Mott transition is characterized by $z = 4$. This is contrasted with non-interacting fermion systems on a lattice, where the dynamical exponent z is two[43].

Here, let us see the superfluid-insulator transition in boson systems. The simplest case is the non-interacting boson systems. In this case, the chemical potential is constant regardless of the density of bosons, because all bosons have zero momentum. Thus, the superfluid-insulator transition is trivial. Then, what about interacting boson systems on a lattice? For simplicity, we consider the hard-core boson model on a hypercubic lattice. A superfluid-insulator transition occurs when the boson density n reaches 1. (Due to the particle-hole transformation, $n \to 1$ is equivalent to $n \to 0$.) In two dimensions, near the transi-

tion point ($n \to 0$), the doping dependence of the chemical potential is asymptotically linear with logarithmic corrections as $\mu \propto n/|\ln \mu|$[82]. This logarithmic correction leads to the divergence of the charge susceptibility near the transition point as $\chi_c \propto [\partial\mu/\partial n]^{-1} \propto |\ln n|$.

Next, we would like to see the case where a superfluid-insulator transition occurs at $n(\neq 0, 1)$. As the simplest case, we consider the hard-core boson model with nearest neighbor repulsion on a square lattice defined as

$$\mathcal{H} = t\sum_{\langle i,j\rangle}(b_i^\dagger b_j + b_j^\dagger b_i) + 4V\sum_{\langle i,j\rangle}(n_i - 1/2)(n_j - 1/2), \tag{6.1}$$

where $b_i^\dagger$ is the creation operator of a hard-core boson at site i, and $n_i \equiv b_i^\dagger b_i$. This model is nothing but the spin-1/2 XXZ model[83]. For $V < t/2$, the ground state is believed to have the off-diagonal long-range order[1]. At $V = t/2$, i.e. the SU(2) symmetric point (XXX model), it is believed that the ground state has the antiferromagnetic long-range order[85]. Thus, there is a gapless excitation at this point, due to the Goldstone theorem[86]. For the Ising-like anisotropic case ($V > t/2$), an excitation gap opens. Hence, the superfluid-insulator transition occurs at half-filling in the language of the hard-core boson model.

Also, as shown in Sec. 5.1, the spin-1/2 XXZ model with Ising-like anisotropy corresponds to the effective model of the $U \to -\infty$ Hubbard model with nearest neighbor repulsion. Thus, by investigating the magnetization process of the Ising-like spin-1/2 XXZ model, we can obtain information about the superconductor-insulator transition in the $U \to -\infty$ Hubbard model with nearest neighbor repulsion. Hence, we investigate the magnetization process of the Ising-like spin-1/2 XXZ models in two and three dimensions, and compare it with the one-dimensional case and the classical-spin case.

This chapter is organized as follows: In Sec. 6.2, the XXZ model is defined. The details of the numerical method are presented. (See also Appendix A.4.) In Sec. 6.3, we review the magnetization process of the

[1]For $0 \leq 2V/t < 0.13$, the presence of the off-diagonal long-range order in the ground state is rigorously proved in Ref.[84].

classical Ising-like XXZ model. In Sec. 6.4, we show numerical results on the magnetization curve of the spin-1/2 Ising-like XXZ models (I-XXZ models) in two and three dimensions. In Sec. 6.5, the behavior of the magnetization curve in the Ising-limit is investigated by means of perturbation theory. In Sec. 6.6, we summarize this chapter.

6.2 Model and method

In the present chapter, we consider the XXZ model defined by the following Hamiltonian:

$$\mathcal{H}_{XXZ} = J \sum_{\langle i,j \rangle} (S_i^x S_j^x + S_i^y S_j^y + \lambda S_i^z S_j^z), \tag{6.2}$$

where $S_i^{x(y,z)}$ denote the $x(y,z)$ components of the spin operator at site i. Here $\langle i,j \rangle$ denotes nearest neighbors. The anisotropic coupling constant is denoted by λ. For $\lambda = 1$, the isotropic Heisenberg model is recovered. We investigate the spin-1/2 I-XXZ models on square and cubic lattices in the ground state in the canonical ensemble. Namely, we measure the energy E within the subspace of fixed magnetization M $(=\sum_i S_i^z)$. The magnetic field in a finite-size cluster is defined as $H(M) \equiv (E(M_1) - E(M_2))/(M_1 - M_2)$, where M is defined by $(M_1 + M_2)/2$. In the thermodynamic limit, this definition of the magnetic field reduces to the normal one: $H \equiv \partial E/\partial M$. The maximum magnetization and the saturation field are denoted by $M_{\max}(=N_s/2)$ and $H_{\max}(=J(\lambda+1)d)$, respectively. Here, N_s and d are the system size and the spatial dimensionality.

We use the Lanczos algorithm (exact diagonalization) for clusters up to 32 sites and the cluster algorithm[87] (quantum Monte Carlo) for larger clusters up to 100 sites. For the cluster algorithm, the measurements have been performed at the inverse temperature $\beta J = 16$. The width of the Trotter slice is chosen as $\Delta\tau J = 0.04$ for two dimensions (2d) and $\Delta\tau J = 0.053$ for three dimensions (3d). The simulation has been performed in the canonical ensemble. In the small-λ regime, the number of points near $M = 0$ obtained by exact diagonalization is too small to use the Maxwell construction. On the other hand, in the

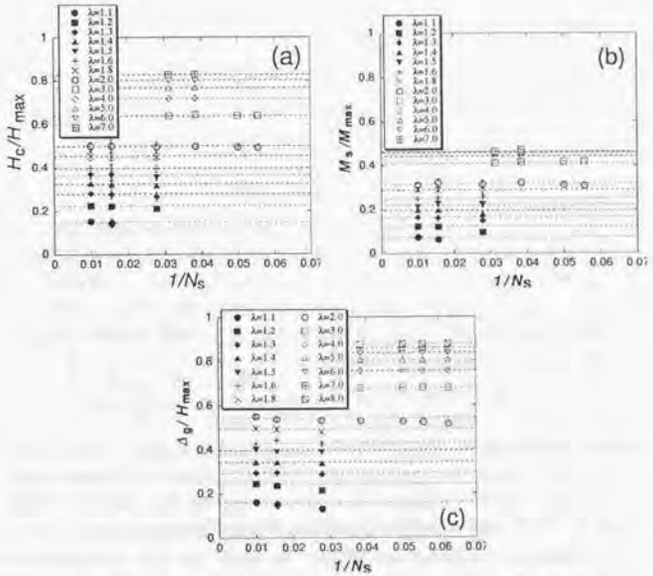

Figure 6.1: Size dependence of the critical field H_c [(a)], the magnetization jump M_s [(b)] and the energy gap [(c)] Δ_g on the two-dimensional spin-1/2 XXZ model. Dotted lines are guides to the eye.

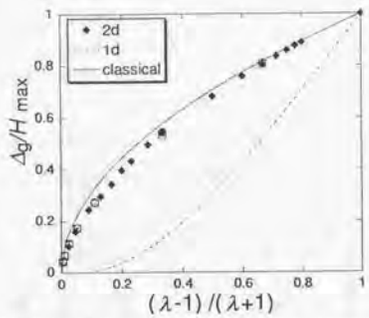

Figure 6.2: Energy gap Δ_g for the two-dimensional spin-1/2 XXZ model. Open circles and open squares denote the results obtained by third-order spin-wave theory cited from [88] and the series expansion cited from [89], respectively. Solid and dotted lines correspond to the classical and one-dimensional cases, respectively.

large-λ regime, statistical errors in the quantum Monte Carlo calculation become large, because the spin configurations are almost frozen. Hence, we have investigated the small-λ regime by quantum Monte Carlo and the large-λ regime by exact diagonalization.

In order to see finite-size effects, we show the size-dependence of the energy gap $\Delta_g(\equiv E(M=1)-E(M=0))$, the critical field H_c and the magnetization jump M_s in Fig. 6.1. The critical field H_c is defined as the magnetic field above which the ground state has non-zero magnetization. As shown in this figure, the size-dependence is very small. As a check of numerical accuracy, we compare the energy gap Δ_g obtained by this method with those obtained by other methods as shown in Fig. 6.2. Our result is quite consistent with those of third-order spin-wave theory[88] and the series expansion around the Ising-limit[89]. Hence, we consider that the inverse temperature β and the width of the Trotter slice $\Delta\tau$ are sufficient. [See also Fig. 6.4.] For

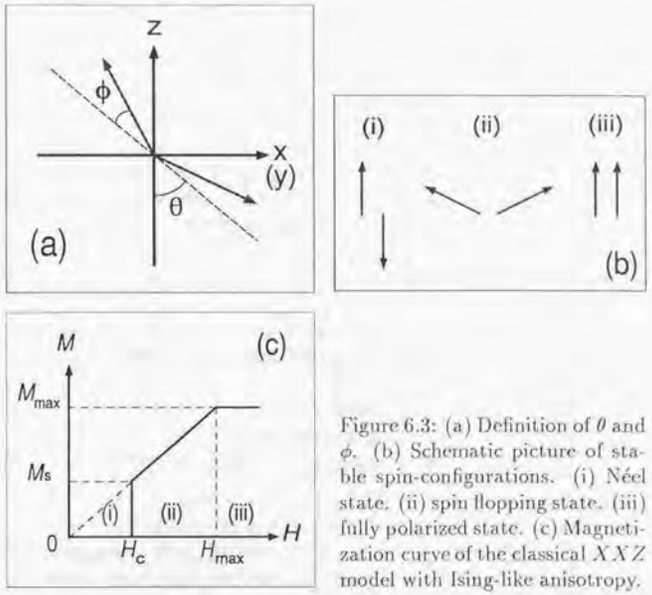

Figure 6.3: (a) Definition of θ and ϕ. (b) Schematic picture of stable spin-configurations. (i) Néel state. (ii) spin flopping state. (iii) fully polarized state. (c) Magnetization curve of the classical XXZ model with Ising-like anisotropy.

three dimensions, we report the 64-site results.

6.3 Classical spin case

Before investigating the spin-1/2 XXZ models, we briefly review the magnetization process of the classical I-XXZ model in the ground state[90, 91]. The ground state energy of the classical I-XXZ model may be written in the following form:

$$E_{C-XXZ} = \frac{JN_s z}{2}(S_A^x S_B^x + S_A^y S_B^y + \lambda S_A^z S_B^z)$$

$$= -\frac{JN_s zS^2}{2}(\sin(\theta+\phi)\sin(\theta-\phi) + \lambda\cos(\theta+\phi)\cos(\theta-\phi)), \tag{6.3}$$

where $S_{A(B)}^{x(y,z)}$ represent the $x(y,z)$ components of the spin operators at a site in the A(B) sublattices. The length of the spin and the coordination number are denoted by S and $z(=2d)$, respectively. The angles θ and ϕ are defined as in Fig. 6.3(a) ($0 \le \theta \le \pi/2$, $0 \le \phi \le \pi/2$). The Zeeman term E_Z is written in the following form:

$$E_Z = -\frac{HN_s}{2}(S_A^z + S_B^z) = \frac{HN_sS}{2}(\cos(\theta+\phi) - \cos(\theta-\phi)). \tag{6.4}$$

By minimizing the total energy ($E_{tot} \equiv E_{C-XXZ} + E_Z$) with respect to θ and ϕ, one finds the following stable states (Fig. 6.3(b)):

(i) $\theta = 0$, $\phi = 0$,
$E_{tot} = -\tilde{J}\lambda$ for $\tilde{H} < \tilde{J}\sqrt{\lambda^2-1}$

(ii) $\theta = \pi/2$, $\phi = \arcsin\frac{\tilde{H}}{\tilde{J}(\lambda+1)}$,
$E_{tot} = -\tilde{J} - \frac{\tilde{H}^2}{\tilde{J}(\lambda+1)}$ for $\tilde{J}(\lambda+1) > \tilde{H} > \tilde{J}\sqrt{\lambda^2-1}$

(iii) $\theta = \pi/2$, $\phi = \pi/2$,
$E_{tot} = \tilde{J}\lambda - 2\tilde{H}$ for $\tilde{H} > \tilde{J}(\lambda+1)$,

where $\tilde{J}$ and $\tilde{H}$ are defined as $\tilde{J} \equiv JN_szS^2/2$ and $\tilde{H} \equiv HN_sS/2$. The magnetization curve of the classical I-XXZ model is shown in Fig. 6.3(c). The transition from state (i) to state (ii) is known as the spin-flopping process[90, 91]. The critical field H_c is defined as the magnetic field above which the ground state has non-zero magnetization. The λ dependence of the critical field H_c and that of the magnetization jump M_s are obtained as

$$H_c/H_{max} = M_s/M_{max} = \sqrt{(\lambda-1)/(\lambda+1)}, \tag{6.5}$$

where $H_{max} = JSz(\lambda+1)$ and $M_{max} = N_sS$.

6.4 Spin-1/2 XXZ model

In the previous section, we have reviewed the magnetization process of the classical-spin case. The transition in a magnetic field is of first

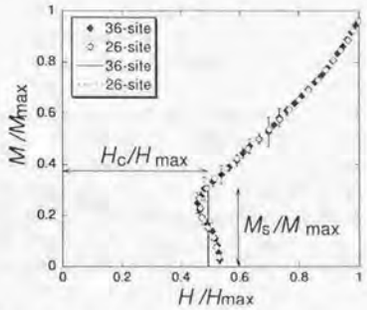

Figure 6.4: Magnetization curve of the two-dimensional spin-1/2 XXZ model with Ising-like anisotropy. Open and solid symbols denote the data in 26-site and 36-site clusters, respectively. Solid (dotted) lines correspond to the phase-separated states determined on the basis of the Maxwell construction by using the data in 36-site (26-site) clusters. We choose $M_1 - M_2 = 1$ or 2 in the definition of the magnetic field H. The definition of the magnetic field H is in the text. The 36-site data for $0 < M/M_{max} < 0.6$ are obtained by quantum Monte Carlo. Other data are obtained by exact diagonalization.

order. A question arising here is how this classical behavior is modified in quantum-spin systems. Thus, in this section, we present the numerical results on the magnetization curve of the spin-1/2 I-XXZ models on square and cubic lattices. As an example, we show the magnetization curve of the spin-1/2 XXZ model for $\lambda = 2$ on a square lattice in Fig. 6.4. The critical field H_c and the magnetization jump M_s are determined on the basis of the Maxwell construction as follows. [See also Fig. 6.9(a).] We fit the energy as a function of magnetization by a polynomial. The tangent from the point at $M = 0$ to the fitting curve gives a lower energy than the numerical data in the region of $0 < M < M_s$. Here, M_s is the magnetization at the point of contact between the fitting curve and the tangent. Hence, we can identify the region of phase separation as $0 < M < M_s$ on the basis of the Maxwell construction. [2] The magnetic field of the phase-separated state (H_c) is given as the slope of the tangent. In practice, we have determined the phase-separation boundary as the point where the following condition is satisfied: $\partial E/\partial M = (E(M) - E(M = 0))/M$ as in Fig. 6.5. The size-dependence of the critical field H_c and that of the magnetization jump M_s determined by the Maxwell construction are very small as shown in Sec. 6.2 (Fig. 6.1).

We show the λ dependence of the critical field H_c in Fig. 6.6. The critical field H_c is suppressed by quantum fluctuations. In order to see how large the critical field H_c is suppressed by quantum fluctuations, we have tried to fit the numerical data as $H_c/H_{\max} = (\frac{\lambda-1}{\lambda+1})^{\alpha}$, analogously with the classical result $\alpha = 0.5$ (eq.(6.5)). We estimate α to be $\alpha = 0.64 \pm 0.01$ for 2d and $\alpha = 0.57 \pm 0.01$ for 3d. Note that the λ dependence of the critical field H_c in two and three dimensions is quite different from the one-dimensional case, where the gap ($= H_c \equiv \partial E/\partial M|_{M/M_{\max} \to +0}$) opens exponentially: $H_c \propto \exp[-\pi^2/2\sqrt{2(\lambda-1)}]$[81].

Here, we mention the relation between the critical field H_c and the energy gap Δ_g. It is expected that the energy gap Δ_g is larger than the critical field H_c, if a first-order transition occurs in the presence of

[2] The finite-size effects on the energy in the phase-separated state may be much larger than those in a homogeneous state because of macroscopic fluctuations. The system sizes examined in this paper may be insufficient to obtain an accurate value for the energy of the phase-separated state. Therefore, we use the Maxwell construction to determine it.

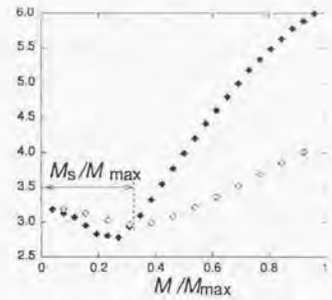

Figure 6.5: $\partial E/\partial M$ (solid symbols) and $(E(M) - E(M = 0))/M$ (open symbols). The intersection point of two curves corresponds to the phase-separation boundary. The data are obtained by exact diagonalization in a 26-site cluster ($\lambda = 2$). We set $J = 1$.

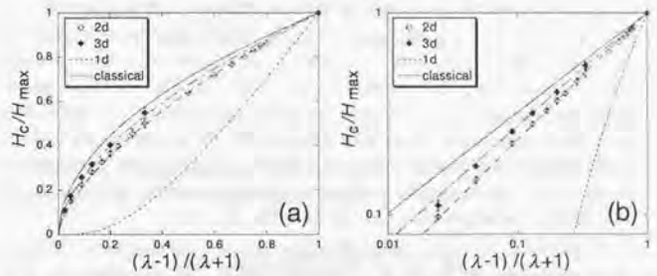

Figure 6.6: Anisotropy λ dependence of the critical field H_c of the spin-1/2 XXZ model. (a) Linear plot and (b) Log-log plot. Solid and dotted lines correspond to the classical and one-dimensional cases, respectively. Dashed and dash-dotted lines correspond to the cases $\alpha = 0.64$ and $\alpha = 0.57$. The definition of α is in the text.

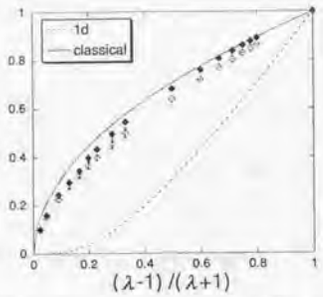

Figure 6.7: Anisotropy λ dependence of the energy gap Δ_g (solid symbols) and the critical field H_c (open symbols) of the spin-1/2 XXZ model on a square lattice. The data are normalized by H_{max}. Solid and dotted lines correspond to the classical and one-dimensional cases, respectively.

a magnetic field. The reason is as follows: The ground state of $M = 1$ is considered to be the one-magnon state, which may be described by spin-wave theory. The gap Δ_g corresponds to the excitation energy of one magnon from the ground state of $M = 0$. On the other hand, phase separation occurs, because magnons gain energy by interacting attractively with each other. The critical field H_c would be determined by the effective attractive interactions between the macroscopic number of magnons. As a result, if phase separation occurs, the gap Δ_g is expected to be larger than the critical field H_c, i.e.

$$\Delta_g > H_c \equiv \partial E/\partial M|_{M/M_{max}\to+0}, \tag{6.6}$$

where M is assumed to be a macroscopic number when the limit $M/M_{max} \to +0$ is taken. We compare the gap Δ_g with the critical field H_c of the spin-1/2 1-XXZ model on a square lattice in Fig. 6.7. The gap Δ_g is always larger than the critical field H_c as expected. It is interesting to contrast this behavior with the one-dimensional result. In one dimension, the transition is of second order[14], and the following relation

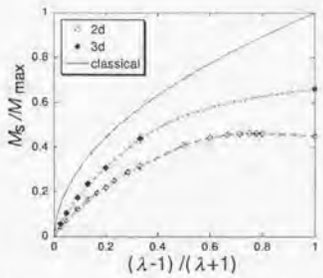

Figure 6.8: Anisotropy λ dependence of the magnetization jump M_s of the spin-1/2 XXZ model. The solid line corresponds to the classical case. Bold lines are guides to the eye. This figure corresponds to the phase diagram of the $U \to -\infty$ Hubbard model with nearest-neighbor repulsion by relating the electron density ρ and the strength of the nearest-neighbor repulsion V/t to M/M_{max} and λ according to $\rho = (1 - M/M_{max})/2$ and $V/t = (\lambda - 1)t/|U|$. The definition of the extended attractive Hubbard model is in Sec. 5.1.

is satisfied: $\partial E/\partial M|_{M/M_{max}\to+0} = E(M = 1) - E(M = 0)$. This is considered to be due to effective repulsive interactions.

The λ dependence of the magnetization jump M_s is shown in Fig. 6.8. We estimate the critical value of λ, at which M_s vanishes, as $\lambda_c = 1.00 \pm 0.02$ by extrapolating the data in Fig. 6.8. This confirms that the spin-1/2 1-XXZ models on square and cubic lattices show a first-order transition at some critical field for any value of the anisotropic coupling constant larger than one ($\lambda > 1$). The λ dependence of the magnetization jump M_s is remarkably different from the classical result, especially in the large-λ regime.

6.5 Ising-limit

In this section, we discuss the magnetization process of the spin-1/2 XXZ model in the Ising-limit. In Fig. 6.8, the value of the magnetization jump M_s in the Ising-limit ($\lambda \to \infty$) does not coincide with that of the Ising model ($M_s = M_{\max}$). This can be explained by means of perturbation theory as follows. We rewrite the spin-1/2 XXZ model as

$$\mathcal{H}_{XXZ} = \bar{J} \sum_{\langle i,j \rangle} S_i^z S_j^z + \epsilon \bar{J} \sum_{\langle i,j \rangle} (S_i^x S_j^x + S_i^y S_j^y), \tag{6.7}$$

where $\bar{J}$ and ϵ are defined as $\bar{J} \equiv J\lambda$ and $\epsilon \equiv 1/\lambda$. We consider the XY-term as the perturbation. At $M = 0$, the unperturbed ground states are the two-degenerate Néel states. The leading perturbation energy is of order ϵ^2. On the other hand, in the limit $M \to M_{\max}$, the leading perturbation energy is of order ϵ and proportional to $M - M_{\max}$. Hence, it is expected that phase separation occurs for the magnetization smaller than some value $M_s (< M_{\max})$ in the Ising-limit. We numerically estimate the value of M_s in the Ising-limit by first-order perturbation theory in the following way. The first-order perturbation energy E_1 is obtained as

$$E_1 = \frac{\epsilon \bar{J}}{2} \frac{\sum_{\alpha,\beta} \langle \beta | \sum_{\langle i,j \rangle} (S_i^+ S_j^- + S_i^+ S_j^-) | \alpha \rangle}{\sum_\alpha \langle \alpha | \alpha \rangle}, \tag{6.8}$$

where $|\alpha\rangle$ and $|\beta\rangle$ denote unperturbed ground states of the Ising model in the subspace of fixed magnetization. We generate $|\alpha\rangle$'s randomly and measure E_1 using a Monte Carlo technique. The value of M_s is determined based on the Maxwell construction. Figure 6.9 shows the first-order perturbation energy E_1 and the value of M_s in the Ising-limit on hyper-cubic lattices in dimensions up to six. We extrapolate the data in Fig. 6.9(b) and estimate the inverse dimensionality, where M_s coincides with $M_{\max}$, as $1/d = 0.01 \pm 0.02$. This confirms that the value of M_s in the Ising-limit ($\lambda \to \infty$) does not coincide with that of the Ising model in finite spatial dimensions.

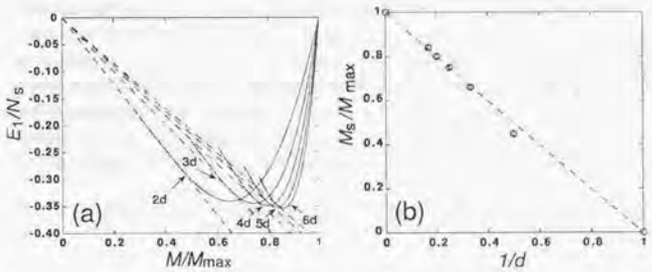

Figure 6.9: (a) First-order perturbation energy in the Ising-limit on hyper-cubic lattices. We set $J = 1$ as the energy unit. The system sizes are 400 sites for 2d, 1000 sites for 3d, 1296 sites for 4d, 1024 sites for 5d and 4096 sites for 6d. Dashed lines denote the tangents from $M = 0$. The magnetization at the point of contact corresponds to M_s. (b) Dimensionality d dependence of M_s in the Ising-limit on hyper-cubic lattices. The dashed line represents $M_s/M_{\max} = 1/d$.

6.6 Summary and discussion

In this section, we translate the numerical results for the spin-1/2 XXZ model with Ising-like anisotropy to the language of the extended attractive Hubbard model. Figure 6.8 corresponds to the ground-state phase diagram of the attractive model with nearest-neighbor repulsion in the limit $U \to -\infty$. From this figure, we can obtain following features about the superconductor-insulator transition in this extended $U \to -\infty$ Hubbard model: (i) The superconductor-insulator transition is a first-order transition for $V > 0$ in two and three dimensions. (ii) There is a finite region of a homogeneous superconducting state in the low-density regime, however large the interaction strength V is. In other words, in the region of the electron density less than about quarter-filling, phase separation does not occur in two dimensions.

Also, the spin-1/2 XXZ model can be regarded as the strong-coupling limit ($U = \infty$) of the following extended Bose-Hubbard model:

$$\mathcal{H}_{\rm BH} = t\sum_{\langle i,j\rangle}(b_i^\dagger b_j + b_j^\dagger b_i) + U\sum_i n_i(n_i - 1) + 4V\sum_{\langle i,j\rangle}(n_i - 1/2)(n_j - 1/2), \tag{6.9}$$

where $b_i^\dagger$ (b_i) creates (annihilates) a boson on site i, and $n_i = b_i^\dagger b_i$. Here $\langle i,j\rangle$ denotes nearest neighbors. The extended Bose-Hubbard models are considered to be relevant for low-temperature properties of liquid helium on a periodic substrate and also for Josephson junction arrays [76, 92, 93]. From the theoretical point of view, a lot of attention has been paid to the Bose-Hubbard model as the simplest model to describe the superfluid-insulator transition [76, 92, 93, 94, 95]. We can also obtain information about the superfluid-insulator transition occurring in the extended Bose-Hubbard model in the strong-coupling limit ($U = \infty$). Figure 6.8 corresponds to the phase diagram of this model by relating the filling ρ and the interaction strength V/t to $M/M_{\rm max}$ and λ according to $\rho = (1 - M/M_{\rm max})/2$ and $V/t = \lambda/2$. The superfluid-insulator transition occurs in the region of $V > t/2$. This transition is a first-order transition, which is consistent with recent investigation of the Bose-Hubbard model[95]. Phase separation does not occur for the density ρ smaller than $\rho_c(\equiv (1 - M_s(\lambda \to \infty)/M_{\rm max})/2 > 0)$. This ρ_c approaches zero as the spatial dimensionality d goes to infinity (Fig.

6.9(b)).

In summary, numerical results on the magnetization process of the spin-1/2 Ising-like XXZ models have been reported. The spin-1/2 XXZ models on square and cubic lattices show a first-order phase transition in a magnetic field for the anisotropic coupling constant larger than one ($\lambda > 1$). The critical field H_c and the magnetization jump M_s are estimated on the basis of the Maxwell construction. The critical field H_c is suppressed by quantum fluctuations (Fig. 6.6). We have demonstrated that the energy gap Δ_g is larger than the critical field H_c (Fig. 6.7). The anisotropy λ dependence of the magnetization jump M_s is remarkably different from the classical result (Fig. 6.8). It is strongly suggested that the value of M_s in the Ising-limit ($\lambda \to \infty$) does not coincide with that of the Ising model in finite spatial dimensions due to quantum effects (Fig. 6.9).

Chapter 7

General summary

We have investigated ground-state properties of Hubbard-type models in the strong-coupling limit. In part I, we have considered repulsive Hubbard model in the large-U limit. In part II, we have considered the magnetization process of the spin-$\frac{1}{2}$ Ising-like XXZ models, which corresponds to the superconductor-insulator transition in the attractive Hubbard model in the limit $U \to -\infty$ with nearest-neighbor repulsion. Main results in this thesis are summarized as follows:

1. We have demonstrated, by analytical and numerical approaches, that ferromagnetism can be realized in the ground state of the Hubbard model on a bipartite lattice for *finite hole-density*.

2. We have shown, by the density-matrix renormalization method and by the analysis of the ground-state spectral flow, that a charge gap opens for the $U = \infty$ Hubbard ladder at quarter-filling for $|t_\perp/t| > 0.001$. (We infer that a charge gap probably opens for $t_\perp/t \neq 0$.)

3. We have confirmed numerically that the magnetization process of the spin-$\frac{1}{2}$ Ising-like XXZ models on square and cubic lattices is a first-order transition.

4. We have shown, by a perturbative argument and numerical calculations, that the magnetization jump in the Ising-limit of the spin-$\frac{1}{2}$ XXZ model does not coincide with that of the Ising model in finite spatial dimensions.

In this thesis, we have focused our attention on itinerant ferromagnetism, the metal-insulator transition and the superfluid-insulator transition in Hubbard-type models. Although we have treated simplified models in the strong-correlation limit, we consider that some features in these models are common to various models with strong correlations. This is because simplified models such as the $U = \infty$ Hubbard model and the spin-$\frac{1}{2}$ XXZ model can be regarded as effective models in the strong-correlation limit of various models. For example, the $U = \infty$ Hubbard model can also be regarded as an effective model of the Kondo lattice model in the limit of the large Kondo-coupling J_K. Also, the spin-$\frac{1}{2}$ Ising-like XXZ model can be regarded as the Bose-Hubbard model with nearest-neighbor repulsion in the hard-core limit.

We would like to end this thesis with short remarks: (1) We have considered effective models derived perturbatively in the strong-coupling limit. Hence, it is expected that the original models in the strong-coupling regime share qualitatively the same features with the effective models. However, arguments are justified only in the limit. Careful analysis is required for finite values of couplings. (2) It is also true that, in strongly correlated systems, there are a lot of phenomena, which are much more complicated and difficult to understand from weak-coupling and strong-coupling expansions.

Appendices

A.1 Derivation of the t-J model

In this appendix, we review a realistic derivation of the t-J model for high-T_c superconductors, following the paper by Zhang and Rice[22].

We consider the copper oxide plane described by the following Hamiltonian:

$$\begin{aligned}
\mathcal{H}_{\mathrm{CuO}} &\equiv \mathcal{H}_d + \mathcal{H}_p + \mathcal{H}_d^U + \mathcal{H}_{dp}, \\
\mathcal{H}_d &\equiv \sum_{i,\sigma} \epsilon^d n_{i\sigma}^d, \\
\mathcal{H}_p &\equiv \sum_{i,\sigma} \epsilon^p n_{i\sigma}^p, \\
\mathcal{H}_d^U &\equiv U \sum_i d_{i\uparrow}^\dagger d_{i\uparrow} d_{i\downarrow}^\dagger d_{i\downarrow}, \\
\mathcal{H}_{dp} &\equiv \sum_{i,\sigma} \sum_{l \in \{i\}} V_{il} d_{i\sigma}^\dagger p_{l\sigma} + \mathrm{h.c.}.
\end{aligned} \tag{A.1.1}$$

where number operators $n_{i\sigma}^d$ and $n_{i\sigma}^p$ are defined as $n_{i\sigma}^d \equiv d_{i\sigma}^\dagger d_{i\sigma}$ and $n_{i\sigma}^p \equiv p_{i\sigma}^\dagger p_{i\sigma}$, respectively. Here, $d_{i\sigma}^\dagger$ and $p_{i\sigma}^\dagger$ represent creation operators of a Cu ($3d_{x^2-y^2}$) hole and an O ($2p_x, 2p_y$) hole at site i, respectively. The on-site Coulomb repulsion at a Cu site is denoted by U. We set the atomic energy of Cu holes $\epsilon_d = 0$, and consider the case $\epsilon_p > 0$. The vacuum is defined as filled Cu d^{10} and O p^6 states.

At half-filling (1 hole/Cu), at $V_{il} = 0$, all the Cu sites are singly occupied, and all the O sites are empty in the hole representation. Here, we consider the case $|V_{il}| \ll U, \epsilon^p, U - \epsilon^p$. At half-filling, the

effective Hamiltonian is derived by means of second-order perturbation theory as

$$\mathcal{H}_S = J \sum_{\langle i,j \rangle} \boldsymbol{S}_i \cdot \boldsymbol{S}_j, \quad J = \frac{4V^4}{\epsilon^{p2} U} + \frac{4V^4}{2\epsilon^{p3}}, \tag{A.1.2}$$

where $\boldsymbol{S}_i$ is a spin-1/2 operator of Cu holes at site i, and $V = |V_{il}|$. Here, $\langle i, j \rangle$ denotes nearest neighbors.

Upon doping, in the atomic limit $V \to 0$, the additional holes sit either at Cu sites if $\epsilon^p > U$, or O sites if $\epsilon^p < U$. The former case reduces to a single band Hubbard model, because the physics is determined by the hole motion on Cu sites. In the following, we consider the latter case ($\epsilon^p < U$). Let us consider a 5-site system composed of four O sites and a Cu ion in the center. Assuming that the strength of hybridization is small ($|V_{il}| \ll U, \epsilon^p, U - \epsilon^p$), we obtain following single-hole states by second-order perturbation theory: (i) a singlet state with energy $-8(t_1 + t_2)$, (ii) triplet states with energy $-8(t_1 + t_2)$, and (iii) non-bonding states with energy $-4t_1$, where $t_1 \equiv V^2/\epsilon^p$ and $t_2 \equiv V^2/(U - \epsilon^p)$. The states (i) and (ii) are symmetric states with respect to the central Cu ion, and the state (iii) is an anti-symmetric state. We neglect states (ii) and (iii), and construct a complete and orthogonal set of O-hole states $\phi_{i\sigma}$ composed of state (i). The O-hole states $\phi_{i\sigma}$ form a spin-singlet state ($-$) and a triplet state ($+$) with the Cu hole at site i:

$$\psi_i^\pm \equiv \frac{1}{\sqrt{2}} (\phi_{i\uparrow} d_{i\downarrow} \pm \phi_{i\downarrow} d_{i\uparrow}). \tag{A.1.3}$$

Here, the triplet state has higher energy than the spin-singlet state. Hereafter, we consider the system within the singlet $\{\psi_i^-\}$ subspace. Since the O holes are created in the background with singly-occupied Cu holes, the motion of a spin-singlet state $\{\psi_i^-\}$ from site i to j is equivalent to that of a Cu hole from site j to i. Thus, the effective hopping Hamiltonian reduces to the following form:

$$\mathcal{H}_t \equiv t \sum_{\langle i,j \rangle \sigma} (\tilde{d}_{i\sigma}^\dagger \tilde{d}_{j\sigma} + \mathrm{h.c.}), \tag{A.1.4}$$

where $\tilde{d}_{i\sigma}^\dagger$ is a creation operator of a Cu hole at site i with the constraint that two Cu holes cannot reside at site i, or $\tilde{d}_{i\sigma}^\dagger \equiv (1 - n_{i-\sigma}) d_{i\sigma}^\dagger$. Hence,

the effective Hamiltonian derived from Hamiltonian $\mathcal{H}_{CuO}$ is nothing but the Hamiltonian of the single-band t-J model $\mathcal{H}_{tJ}$.

A.2 DMRG method

In this appendix, we briefly review the density-matrix renormalization group (DMRG) method proposed by White[35]. As an example, we consider the $U = \infty$ Hubbard ladder.

A.2.1 Infinite-system algorithm

As an initial step, the Hamiltonian $\mathcal{H}$, the creation operator at rung 2 $\tilde{c}^{\alpha}_{2\sigma}$ and the number operator $\mathcal{N}_\sigma$ of the 4-state system are constructed in the site representation. Here, α is the suffix for legs ($\alpha = 1, 2$), and σ denotes the z-component of the spin ($\sigma = \uparrow, \downarrow$).

Next, we construct the Hamiltonian of the 8-site system from the operators of the 4-site system, as represented in Fig. A.2.1. The ground-state wavefunction $|\mathrm{GS}\rangle$ of the 8-site system is obtained by the Lanczos method. Here, $|\mathrm{GS}\rangle$ is expressed in the site representation as $|\mathrm{GS}\rangle = \sum_k a_k |k\rangle$, where $|k\rangle$ denotes a basis of the site representation.

Next, we diagonalize the density matrix ρ_{ij} defined as eq.(A.2.5) by, for example, the Householder algorithm.

$$\rho_{ij} \equiv \sum_l a^*_{(i,l)} a_{(j,l)}, \tag{A.2.5}$$

where $i(j)$ and l represent degrees of freedom of legs 1 and 2 and those of legs 1′ and 2′, respectively. We denote by R the matrix which changes the bases from the site representation to the representation in which the density matrix ρ_{ij} is diagonalized. Here, we choose eigenvectors of m largest eigenvalues. The rectangular matrix that truncates the density matrix is denoted by T. Using these matrices R and T, the operators written in the site representation are rewritten in the representation in which the density matrix ρ_{ij} is diagonalized. The matrices representing the operators are truncated to the matrices of size $m \times m$.

The Hamiltonian $\mathcal{H}$ and the number operator $\mathcal{N}_\sigma$ of the 4-site cluster and the creation operators at rung 2 ($\tilde{c}^{\alpha}_{2\sigma}$) written in the site representation are transformed by the matrix TR. The Hamiltonian of a 12-site

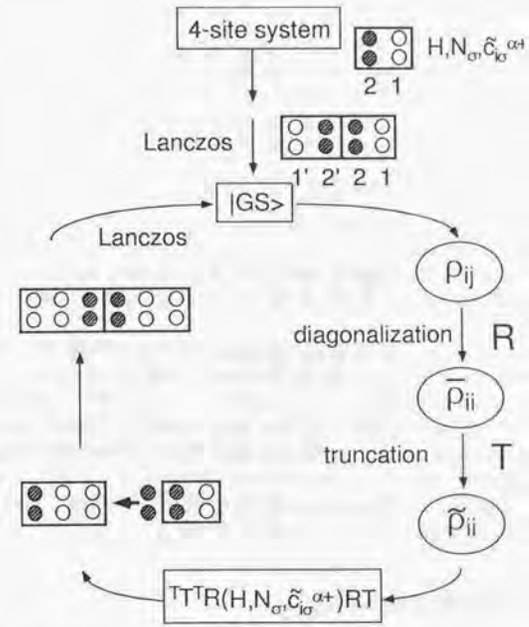

Figure A.2.1: Flow chart of the infinite-system algorithm. Circles represent sites.

cluster is constructed from these operators, where the number of up and down spins are chosen such that the filling and the magnetization are close to the required values. The ground-state wavefunction $|GS\rangle$ of this Hamiltonian is obtained by the Lanczos algorithm.

Repeating the above procedure, we obtain Hamiltonians of large-size systems with the matrix-size fixed on $m \times m$. The Hamiltonians are exact if m is taken as large as the size of the density matrix in each iteration. In practice, m is taken some large number in order to keep accuracy.

A.2.2 Finite-system algorithm

Repeating the above procedure, we obtain an approximate Hamiltonian of the required size of the system. However, this Hamiltonian is sometimes far from the true Hamiltonian especially for electron systems. White proposed the algorithm to improve the approximate Hamiltonian[35].

We construct an N_s-site Hamiltonian from the $N_s/2$-site Hamiltonian and the $(N_s/2-4)$-site Hamiltonian obtained by the infinite-system algorithm. Following the procedure of the infinite-system algorithm, we obtain the $(N_s/2+2)$-site Hamiltonian. Combining this Hamiltonian with the previously obtained $(N_s/2-6)$-site Hamiltonian, we can construct an N_s-site Hamiltonian. Repeating this procedure as shown in Fig. A.2.2, we can successively improve the Hamiltonian with the system-size fixed.

A.3 Hyperscaling

In this appendix, we briefly review the hyperscaling theory proposed by Fisher, *et.al.* for the superfluid-insulator transition[76], and applied by Imada to the metal-insulator transition[43].

We consider the partition function Z defined as

$$Z \equiv \int \mathcal{D}\Phi(\boldsymbol{r},\tau)\mathcal{D}\Phi^*(\boldsymbol{r},\tau)e^{-S}, \qquad \text{(A.3.6)}$$

$$S \equiv \int_0^\beta d\tau[\int_V d\boldsymbol{r}\Phi^*\partial_\tau\Phi + \mathcal{H}],$$

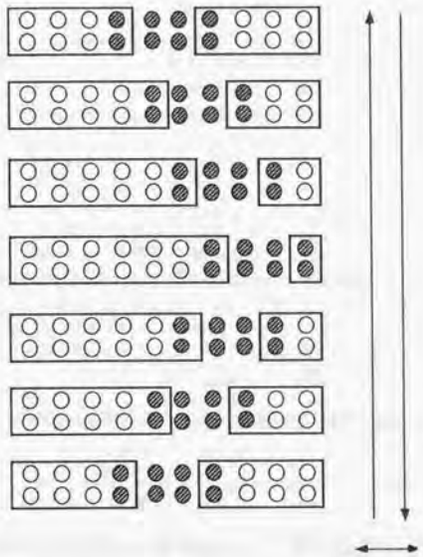

Figure A.2.2: Flow chart of the finite-system algorithm. At the bottom of the flow chart, the system is reversed right-side left.

where $\mathcal{H}$, V and β denote the Hamiltonian, the volume in the d-dimensional space ($\equiv L^d$) and the inverse temperature($\equiv 1/T$), respectively. The Grassman field $\Phi(\boldsymbol{r},\tau)$ is defined in the $(d+1)$-dimensional space-time. The free energy per volume f is defined as

$$f \equiv -\frac{1}{\beta V}\ln Z. \tag{A.3.7}$$

In the following, we consider the limit $\beta \to \infty$ ($T \to 0$) and $L \to \infty$. We introduce fermion creation (annihilation) operators $a^\dagger(\boldsymbol{r},\tau)(a(\boldsymbol{r},\tau))$ in the second quantized form. A twist of the boundary condition in the imaginary time direction corresponds to the transformation of the fermion operators $a^\dagger(\boldsymbol{r},\tau)$ as

$$a^\dagger(\boldsymbol{r},\tau) \to a^\dagger(\boldsymbol{r},\tau)\exp[i\tau\dot{\phi}]. \tag{A.3.8}$$

The total twist ϕ_β between $\tau = 0$ and $\tau = \beta$ is $\phi_\beta = \beta\dot{\phi}$.

The partition function Z introduced in eq.(A.3.6) may be rewritten as

$$Z = \lim_{\Delta\tau\to 0}\sum_{|\phi_0\rangle}\langle\phi_0|\prod_{m=1}^{M-1}(\mathrm{e}^{-\Delta\tau\mathcal{H}}\sum_{|\phi_m\rangle}|\phi_m\rangle\langle\phi_m|)\mathrm{e}^{-\Delta\tau\mathcal{H}}|\phi_0\rangle, \tag{A.3.9}$$

where $\Delta\tau \equiv \beta/M$. The transformation eq.(A.3.8) is equivalent to the transformation

$$\exp(-\Delta\tau\mathcal{H})|\phi_m\rangle \to \exp(-\Delta\tau[\mathcal{H} + \mathrm{i}\dot{\phi}\sum_{\boldsymbol{r}} a^\dagger(\boldsymbol{r},\tau)a(\boldsymbol{r},\tau)])|\phi_m\rangle, \tag{A.3.10}$$

where the Hamiltonian $\mathcal{H}$ is assumed to commute with the number operator $\hat{N}_e(\tau) \equiv \sum_{\boldsymbol{r}} a^\dagger(\boldsymbol{r},\tau)a(\boldsymbol{r},\tau)$. Thus, $-\mathrm{i}\dot{\phi}$ plays the role of an additional change in the chemical potential μ. The difference of the free energy density δf, defined as $\delta f \equiv f(\dot{\phi}) - f(\dot{\phi} = 0)$, can be expanded as

$$\delta f = \mathrm{i}\frac{\phi_\beta}{\beta}\rho + \frac{\phi_\beta^2}{2\beta^2}\kappa + O(\phi_\beta^3). \tag{A.3.11}$$

The coefficients ρ and κ are defined as

$$\rho \equiv -\partial f/\partial\mu = \langle a^\dagger(\boldsymbol{r},\tau)a(\boldsymbol{r},\tau)\rangle, \tag{A.3.12}$$

$$\kappa \equiv -\partial\rho/\partial\mu. \tag{A.3.13}$$

Let us discuss the Mott transition based on the scaling hypothesis. We introduce a parameter Δ which measures the distance from the critical point. As an example of Δ, we take the chemical potential measured from that of the critical point, i.e. $\Delta = |\mu - \mu_c|$. We define exponent ν as

$$\xi \propto \Delta^{-\nu}, \tag{A.3.14}$$

assuming that the single length scale ξ diverges as $\Delta \to 0$. The dynamical exponent z, which relates the length scale ξ to the energy scale Ω, is defined as

$$\Omega \propto \xi^{-z}. \tag{A.3.15}$$

When the free energy density f is singular at $\Delta = 0$, the hyperscaling leads the singular part $f_s(\Delta)$ to the form

$$f_s(\Delta) \sim b^{-d+z} f_s(b^{1/\nu}\Delta) \sim \Delta^{\nu(d+z)}, \tag{A.3.16}$$

due to the homogeneity for arbitrary scale transformation parameter b. When both inverse temperature β and linear spatial dimension L are large but finite, the finite-size scaling is expected to be satisfied as

$$f_s(\Delta) \sim \Delta^{\nu(d+z)}\mathcal{F}(\xi/L, \Omega/\beta), \tag{A.3.17}$$

where $\mathcal{F}$ is an appropriate scaling function. Comparing eq.(A.3.17) with eq.(A.3.11), we obtain the asymptotic form of κ to the critical point as

$$\kappa \propto \Delta^{-\nu(z-d)}. \tag{A.3.18}$$

On the other hand, by its definition eq.(A.3.13) and eq.(A.3.17), κ behaves as

$$\kappa \propto \Delta^{\nu(d+z)-2}. \tag{A.3.19}$$

Hence, comparing the above two equations, we obtain

$$\nu z = 1. \tag{A.3.20}$$

The doping δ is defined as the filling ρ measured from the critical point, or $\delta \equiv |\rho - \rho_c|$. Under the assumption of scaling theory, δ behaves near the critical point as

$$\delta \propto \Delta^{\nu(d+z)-1}, \tag{A.3.21}$$

by the definition of ρ in eq.(A.3.12) and eq.(A.3.17). Thus, we obtain the doping dependence of ξ near the critical point as

$$\xi \propto \delta^{-1/d}, \tag{A.3.22}$$

where we have used relations eqs.(A.3.14), (A.3.20) and (A.3.21). Equation (A.3.22) implies that ξ is determined by the mean hole distance. Comparing eqs.(A.3.19), (A.3.20) and (A.3.21), we obtain the doping dependence of κ as

$$\kappa \propto \delta^{1-z/d}. \tag{A.3.23}$$

A.4 Cluster algorithm

In this appendix, we review the quantum Monte Carlo method (cluster algorithm)[87].

By the Suzuki-Trotter transformation, d-dimensional quantum systems are mapped onto $(d+1)$-dimensional classical systems. The partition function Z of quantum systems is written as follows:

$$\begin{aligned} Z &\equiv \sum_{\alpha_1} \langle \alpha_1 | e^{-\beta \mathcal{H}} | \alpha_1 \rangle && \text{(A.4.24)} \\ &= \sum_{\alpha_1} \cdots \sum_{\alpha_M} \Pi_{i=1}^{M} \langle \alpha_i | e^{-\frac{\beta}{M}\mathcal{H}} | \alpha_{i+1} \rangle && \text{(A.4.25)} \\ &= \sum_{A} W(A) + O(1/M), && \text{(A.4.26)} \end{aligned}$$

where $\alpha_{M+1} = \alpha_1$, and $W(A) = \Pi_{i=1} w(a_i)$. Here, A and a_i denote a configuration of Ising-spins in the $(d+1)$-dimensional space-time and the configuration of 4 Ising-spins on plaquette i, respectively. The Boltzmann weight on plaquette i is denoted by $w(a_i)$.

In the following, we consider the spin-1/2 XXZ model as an example. The Hamiltonian is defined as

$$\mathcal{H}_{XXZ} = J \sum_{\langle i,j \rangle} (S_i^x S_j^x + S_i^y S_j^y + \lambda S_i^z S_j^z). \tag{A.4.27}$$

For the spin-1/2 XXZ model, a_i and $w(a_i)$ are explicitly written as

$$\{a_i\} = \left\{ \begin{matrix} \uparrow\uparrow \\ \uparrow\uparrow \end{matrix}, \begin{matrix} \uparrow\downarrow \\ \downarrow\uparrow \end{matrix}, \begin{matrix} \uparrow\downarrow \\ \uparrow\downarrow \end{matrix}, \begin{matrix} \downarrow\uparrow \\ \downarrow\uparrow \end{matrix}, \begin{matrix} \downarrow\uparrow \\ \uparrow\downarrow \end{matrix}, \begin{matrix} \downarrow\downarrow \\ \downarrow\downarrow \end{matrix} \right\}, \tag{A.4.28}$$

	$\sigma_i^x\sigma_j^x + \sigma_i^y\sigma_j^y$	$\sigma_i^z\sigma_j^z$	Λ
$\begin{matrix}\uparrow\uparrow \\ \uparrow\uparrow\end{matrix}, \begin{matrix}\downarrow\downarrow \\ \downarrow\downarrow\end{matrix}$	0	1	λ
$\begin{matrix}\uparrow\downarrow \\ \uparrow\downarrow\end{matrix}, \begin{matrix}\downarrow\uparrow \\ \downarrow\uparrow\end{matrix}$	0	-1	$-\lambda$
$\begin{matrix}\uparrow\downarrow \\ \downarrow\uparrow\end{matrix}, \begin{matrix}\downarrow\uparrow \\ \uparrow\downarrow\end{matrix}$	2	0	2

Table A.4.1: Weight of the local Hamiltonian Λ.

$$w(a_i) = \begin{pmatrix} a & 0 & 0 & 0 \\ 0 & b & c & 0 \\ 0 & c & b & 0 \\ 0 & 0 & 0 & a \end{pmatrix} \begin{matrix} |\uparrow\uparrow\rangle \\ |\uparrow\downarrow\rangle \\ |\downarrow\uparrow\rangle \\ |\downarrow\downarrow\rangle \end{matrix}, \tag{A.4.29}$$

where $a = \exp(-\Delta\tau\lambda J/4)$, $b = \exp(\Delta\tau\lambda J/4)\cosh(\Delta\tau J/2)$ and $c = \exp(\Delta\tau\lambda J/4)\sinh(\Delta\tau J/2)$.

Thus, a_i's can be classified into three groups according to the values of $w(a_i)$. The weights of the local Hamiltonian Λ defined by eq.(A.4.30) are shown in table A.4.1.

$$\Lambda \equiv \sigma_i^x\sigma_j^x + \sigma_i^y\sigma_j^y + \lambda\sigma_i^z\sigma_j^z, \tag{A.4.30}$$

where $\sigma^{x(y,z)}$ denote the $x(y,z)$ components of the vector of the Pauli matrices. Here, we introduce graphs to represent the local Hamiltonian Λ. In the case of the spin-1/2 XXZ model with Ising-like anisotropy, the local Hamiltonian is expressed as eq.(A.4.31) in terms of the graphs $\left(\begin{matrix} | & | \end{matrix}, \begin{matrix} \cdots \\ \cdots \end{matrix}, \text{and} \begin{matrix} | & \begin{matrix} \cdots \\ \cdots \end{matrix} & | \end{matrix} \right)$. Relation between a_i's and the graphs is shown in table A.4.2.

$$\Lambda = \lambda \cdot \begin{matrix} | & | \end{matrix} + 2 \cdot \begin{matrix} \cdots \\ \cdots \end{matrix} - 2(\lambda+1) \begin{matrix} | & \begin{matrix} \cdots \\ \cdots \end{matrix} & | \end{matrix} \tag{A.4.31}$$

Hence, $w(a_i)$ can be expressed as

$$w(a_i) = \sum_{b_i} v(b_i)\delta(a_i, b_i), \tag{A.4.32}$$

	$\vert\ \vert$	$\begin{smallmatrix}\cdots\\ \cdots\end{smallmatrix}$	$\vert\ \begin{smallmatrix}\cdots\\ \cdots\end{smallmatrix}\ \vert$	Λ
$\begin{smallmatrix}\uparrow\uparrow\\ \uparrow\uparrow\end{smallmatrix}, \begin{smallmatrix}\downarrow\downarrow\\ \downarrow\downarrow\end{smallmatrix}$	1	0	0	λ
$\begin{smallmatrix}\uparrow\downarrow\\ \uparrow\downarrow\end{smallmatrix}, \begin{smallmatrix}\downarrow\uparrow\\ \downarrow\uparrow\end{smallmatrix}$	1	1	1	$-\lambda$
$\begin{smallmatrix}\uparrow\downarrow\\ \downarrow\uparrow\end{smallmatrix}, \begin{smallmatrix}\downarrow\uparrow\\ \uparrow\downarrow\end{smallmatrix}$	0	1	0	2

Table A.4.2: Local Hamiltonian Λ in terms of graphs.

where b_i denotes a graph at plaquette i, and $\delta(a_i, b_i)$ is defined as in table A.4.2. Here, $v(b_i)$ denotes the weight of graph b_i determined by eq.(A.4.32). Equation (A.4.32) is explicitly written as

$$\begin{aligned} w(\begin{smallmatrix}\uparrow\uparrow\\ \uparrow\uparrow\end{smallmatrix}, \begin{smallmatrix}\downarrow\downarrow\\ \downarrow\downarrow\end{smallmatrix}) &= v(\vert\ \ \vert), \\ w(\begin{smallmatrix}\uparrow\downarrow\\ \uparrow\downarrow\end{smallmatrix}, \begin{smallmatrix}\downarrow\uparrow\\ \downarrow\uparrow\end{smallmatrix}) &= v(\vert\ \ \vert) + v(\begin{smallmatrix}\cdots\\ \cdots\end{smallmatrix}) + v(\vert\ \begin{smallmatrix}\cdots\\ \cdots\end{smallmatrix}\ \vert), \qquad \text{(A.4.33)} \\ w(\begin{smallmatrix}\uparrow\downarrow\\ \downarrow\uparrow\end{smallmatrix}, \begin{smallmatrix}\downarrow\uparrow\\ \uparrow\downarrow\end{smallmatrix}) &= v(\begin{smallmatrix}\cdots\\ \cdots\end{smallmatrix}), \end{aligned}$$

where

$$\begin{aligned} w(\begin{smallmatrix}\uparrow\uparrow\\ \uparrow\uparrow\end{smallmatrix}) = w(\begin{smallmatrix}\downarrow\downarrow\\ \downarrow\downarrow\end{smallmatrix}) &= \exp(-\Delta\tau\lambda J/4), \\ w(\begin{smallmatrix}\uparrow\downarrow\\ \uparrow\downarrow\end{smallmatrix}) = w(\begin{smallmatrix}\downarrow\uparrow\\ \downarrow\uparrow\end{smallmatrix}) &= \exp(\Delta\tau\lambda J/4)\cosh(\Delta\tau J/2), \qquad \text{(A.4.34)} \\ w(\begin{smallmatrix}\uparrow\downarrow\\ \downarrow\uparrow\end{smallmatrix}) = w(\begin{smallmatrix}\downarrow\uparrow\\ \uparrow\downarrow\end{smallmatrix}) &= \exp(\Delta\tau\lambda J/4)\sinh(\Delta\tau J/2). \end{aligned}$$

Hence, $v(b_i)$ is obtained as

$$\begin{aligned} v(\vert\ \ \vert) &= \exp(-\Delta\tau\lambda J/4), \\ v(\vert\ \begin{smallmatrix}\cdots\\ \cdots\end{smallmatrix}\ \vert) &= \exp(\Delta\tau(\lambda-2)J/4) - \exp(-\Delta\tau\lambda J/4), \qquad \text{(A.4.35)} \end{aligned}$$

$$v(\begin{smallmatrix}\cdots\\ \cdots\end{smallmatrix}) = \exp(\Delta\tau\lambda J/4)\sinh(\Delta\tau J/2).$$

In terms of the graphs introduced above, the total Boltzmann weight of spin configuration A, i.e. $W(A)(\equiv \prod_i w(a_i))$ is expressed as

$$W(A) = \sum_B V(B)\Delta(A, B), \qquad \text{(A.4.36)}$$

where $V(B)$ is defined as $V(B) \equiv \prod_i v(b_i)$. Here, $\Delta(A, B) = 1$ if graph B is compatible to configuration A, otherwise 0. Next, we express the probability of finding spin configuration A, i.e. $Pr(A)(\equiv W(A)/Z, Z \equiv \sum_A W(A))$ in terms of graph B. By introducing conditional probability $Pr(A|B)$, $Pr(A)$ is written as

$$Pr(A) = \sum_B Pr(A|B)Pr(B), \qquad \text{(A.4.37)}$$

where $Pr(A|B)$ can be chosen as

$$Pr(A|B) = \Delta(A, B)/\sum_A \Delta(A, B). \qquad \text{(A.4.38)}$$

Thus, we obtain $Pr(B)$ as $Pr(B) = V(B)\sum_A \Delta(A, B)/Z$. Due to the detailed balance condition $Pr(B|A)Pr(A) = Pr(A|B)Pr(B)$, the conditional probability $Pr(B|A)$ is obtained as

$$\begin{aligned} Pr(B|A) &= \Delta(A, B)V(B)/W(A) \qquad \text{(A.4.39)} \\ &= \Delta(A, B)V(B)/\sum_{B'} \Delta(A, B')V(B'). \end{aligned}$$

Hence, the local conditional probabilities $Pr(a_i|b_i)$ and $Pr(b_i|a_i)$ can be chosen as

$$\begin{aligned} Pr(a_i|b_i) &= \delta(a_i, b_i)/\sum_{a_i} \delta(a_i, b_i), \qquad \text{(A.4.40)} \\ Pr(b_i|a_i) &= \delta(a_i, b_i)v(b_i)/w(a_i). \end{aligned}$$

In the framework of the cluster algorithm, the spin configurations and graphs are updated alternately, according to probabilities $Pr(a_i|b_i)$ and $Pr(b_i|a_i)$. Graph B is constructed from spin configuration A by choosing b_i's according to $Pr(b_i|a_i)$, where a_i is a part of A. The spins on graph B are reversed with probability 1/2.[1]

[1] If the magnetic field is applied, the probability has to be modified. (See Ref.[87] for details.)

References

[1] L.D. Landau, Soviet Phys. JETP **3**, 169 (1957).

[2] N.F. Mott, Proc. Phys. Soc. **62**, 416 (1949); Can. Journ. Phys. **34**, 1356 (1956); Nuovo Cim. Suppl. **7**, 312 (1958); Phil. Mag. **6**, 287 (1961); *Metal-Insulator Transitions* Second Edition (Taylor & Francis, 1990).

[3] J. Hubbard, Proc. Roy. Soc. (London) A **276**, 238 (1963); A **277**, 237 (1964); A **281**, 401 (1964).

[4] P.W. Anderson, Phys. Rev. **115**, 2 (1959); *Solid State Physics* Vol.14 (edited by F. Seitz and D. Turnbull), Academic Press, 99 (1963).

[5] J.G. Bednorz and K.A. Müller, Z. Phys. B **64**, 189 (1986); C.W. Chu, P.H. Hor, R.L. Meng, L. Gao, Z.J. Huang and Y.Q. Wang, Phys. Rev. Lett. **58**, 405 (1987).

[6] P.W. Anderson, Science **235**, 1196 (1987).

[7] Y. Nagaoka, Phys. Rev. **147**, 392 (1966).

[8] D.J. Thouless, Proc. Phys. Soc. London **86**, 893 (1965).

[9] H. Tasaki, Phys. Rev. B **40**, 9192 (1989).

[10] E.H. Lieb and F.Y. Wu, Phys. Rev. Lett. **20**, 1445 (1968).

[11] V.J. Emery, in *Highly Conductiong One-Dimensional Solids*, edited by J.T. Devreese *et. al.* (Plenum, New York,1979), p.247.

[12] M. Ogata and H. Shiba, Phys. Rev. B **41**, 2326 (1990).

[13] M. Kohno, Phys. Rev. B **56**, 15015 (1997).

[14] C.N. Yang and C.P. Yang, Phys. Rev. **150**, 321 (1966); **150**, 327 (1966); **151**, 258 (1966).

[15] M. Kohno and M. Takahashi, Phys. Rev. B **56**, 3212 (1997).

[16] E.H. Lieb, Phys. Rev. Lett. **62**, 1201 (1989); **62**, 1927 (1989).

[17] W. Marshall, Proc. Roy. Soc. (London) A **232**, 48 (1955).

[18] E.H. Lieb and D. Mattis, J. Math. Phys. **3**, 749 (1962).

[19] M. Takahashi, J. Phys. C **10**, 1289 (1977).

[20] J.E. Hirsh, Phys. Rev. Lett. **54**, 1317 (1985).

[21] C. Gros, R. Joynt and T.M. Rice, Phys. Rev. B **36**, 381 (1987).

[22] F.C. Zhang and T.M. Rice, Phys. Rev. B **37**, 3759 (1988).

[23] C.N. Yang, Phys. Rev. Lett. **19**, 1312 (1967).

[24] H. Bethe, Z. Phys. **71**, 205 (1931); L. Hulthén, Arkiv. Mat. Astron. Fys. **26A**, No.11 (1938).

[25] E. Lieb and D. Mattis, Phys. Rev. **125**, 164 (1962).

[26] M. Takahashi, J. Phys. Soc. Jpn. **51**, 3475 (1982).

[27] K. Kubo and M. Tada, Prog. Theor. Phys. **69**, 1345 (1983); **71**, 479 (1984).

[28] J.A. Riera and A.P. Young, Phys. Rev. B **40**, 5285 (1989).

[29] J.S. Yedidia, Phys. Rev. B **41**, 9397 (1990).

[30] X.Y. Zhang, E. Abrahams and G. Kotliar, Phys. Rev. Lett. **66**, 1236 (1991).

[31] W.O. Putikka, M.U. Luchini and T.M. Rice, Phys. Rev. Lett. **68**, 538 (1992).

[32] W.O. Putikka, M.U. Luchini and M. Ogata, Phys. Rev. Lett. **69**, 2288 (1992).

[33] K. Kusakabe and H. Aoki, J. Phys. Soc. Jpn. **61**, 1165 (1992); Phys. Rev. B **50**, 12991 (1994).

[34] S. Liang and H. Pang, Europhys. Lett. **32**, 173 (1995).

[35] S.R. White, Phys. Rev. Lett. **69**, 2863 (1992); Phys. Rev. B **48**, 10345 (1993).

[36] K. Kubo, J. Phys. Soc. Jpn. **51**, 782 (1982).

[37] K. Kusakabe and H. Aoki, Physica B **194-196**, 217 (1994).

[38] M. Sigrist, H. Tsunetsugu, K. Ueda and T.M. Rice, Phys. Rev. B **46**, 13838 (1992).

[39] B.S. Shastry and B. Sutherland, Phys. Rev. Lett. **65**, 243 (1990).

[40] N. Kawakami and S.-K. Yang, Phys. Rev. Lett. **65**, 3063 (1990); Phys. Rev. B **44**, 7844 (1991).

[41] N. Furukawa and M. Imada, J. Phys. Soc. Jpn. **61**, 3331 (1992).

[42] M. Imada, J. Phys. Soc. Jpn. **62**, 1105 (1993); **63**, 3059 (1994).

[43] M. Imada, J. Phys. Soc. Jpn. **64**, 2954 (1995).

[44] F.F. Assaad and M. Imada, Phys. Rev. Lett. **76**, 3176 (1996).

[45] M. Kohno, Phys. Rev. B **55**, 1435 (1997).

[46] K. Kusakabe and H. Aoki, J. Phys. Soc. Jpn. **65**, 2772 (1996).

[47] R. Arita, K. Kusakabe, K. Kuroki and H. Aoki, J. Phys. Soc. Jpn. **66**, 2086 (1997).

[48] L. Balents and M.P.A. Fisher, Phys. Rev. B **53**, 12133 (1996).

[49] J. Zaanen, G.A. Sawatzky and J.W. Allen, Phys. Rev. Lett. **55**, 418 (1985).

[50] V.J. Emery, S.A. Kivelson and H.Q. Lin, Phys. Rev. Lett. **64**, 475 (1990).

[51] E. Dagotto, A. Moreo, F. Ortolani, D. Poilblanc and J. Riera, Phys. Rev. B **45**, 10741 (1992).

[52] P. Prelovšek and X. Zotos, Phys. Rev. B **47**, 5984 (1993).

[53] D. Poilblanc, Phys. Rev. B **52**, 9201 (1995).

[54] C.S. Hellberg and E. Manousakis, Phys. Rev. Lett. **78**, 4609 (1997).

[55] C.T. Shih, Y.C. Chen and T.K. Lee, cond-mat/9705156.

[56] E.C. Stoner, Proc. Roy. Soc. (London) A **154**, 656 (1936); **165**, 372 (1938).

[57] A. Mielke, J. Phys. A: Math. Gen. **24**, L73 (1991); 3311 (1991); **25**, 4335 (1992); Phys. Lett. A **174** 443 (1993).

[58] H. Tasaki, Phys. Rev. Lett. **69**, 1608 (1992).

[59] B. Douçot and X.G. Wen, Phys. Rev. B **40**, 2719 (1989).

[60] Y. Fang, A.E. Ruckenstein, E. Dagotto and S. Schmitt-Rink, Phys. Rev. B **40**, 7406 (1989).

[61] E.V. Kuz'min, JETP Lett. **57**, 591 (1993).

[62] A. Barbieri, J.A. Riera and A.P. Young, Phys. Rev. B **41**, 11697 (1990).

[63] S.A. Trugman, Phys. Rev. B **42**, 6612 (1990).

[64] G.-S. Tian, Phys. Rev. B **44**, 4444 (1991).

[65] S.-Q. Shen, Z.-M. Qiu and G.-S. Tian, Phys. Lett. A **178**, 426 (1993).

[66] B.S. Shastry, H.R. Krishnamurthy and P.W. Anderson, Phys. Rev. B **41**, 2375 (1990).

[67] A.G. Basile and V. Elser, Phys. Rev. B **41**, 4842 (1990).

[68] W. von der Linden and D.M. Edwards, J. Phys. Cond. Matt. **3**, 4917 (1991).

[69] P. Wurth, G. Uhrig and E. Müller-Hartmann, Ann. Physik **5**, 148 (1996).

[70] T. Hanisch, G.S. Uhrig and E. Müller-Hartmann, preprint(condmat/9707286).

[71] T. Hanisch and E. Müller-Hartmann, Ann. Physik **2**, 381 (1993).

[72] M. Ogata, M.U. Luchini, S. Sorella and F.F. Assaad, Phys. Rev. Lett. **66**, 2388 (1991).

[73] C.S. Hellberg and E. Manousakis, Phys. Rev. B **52**, 4639 (1995).

[74] Y.C. Chen and T.K. Lee, Phys. Rev. B **51**, 6723 (1995).

[75] J.H. Cho, F. Borsa, D.C. Johnston and D.R. Torgeson, Phys. Rev. B **46**, 3179 (1992);F. Borsa, P. Carretta, J.H. Cho, F.C. Chou, Q. Hu, D.C. Johnston, A. Lascialfari, D.R. Torgeson, R.J. Gooding, N.M. Salem and K.J.E. Vos, Phys. Rev. B **52**, 7334 (1995).

[76] M.P.A. Fisher, P.B. Weichman, G. Grinstein and D.S. Fisher, Phys. Rev. B **40**, 546 (1989).

[77] R.J. Birgeneau, D.R. Gabbe, H.P. Jenssen, M.A. Kastner, P.J. Picone, T.R. Thurston, G. Shirane, Y. Endoh, M. Sato, K. Yamada, Y. Hidaka, M. Oda, Y. Enomoto, M. Suzuki and T. Murakami, Phys. Rev. B **38**, 6614 (1988).

[78] A. Ino, T. Mizokawa, A. Fujimori, K.Tamasaku, H. Eisaki, S. Uchida, T. Kimura, T. Sasagawa and K. Kishio, Phys. Rev. Lett. **79**, 2101 (1997).

[79] H. Shiba, Prog. Theor. Phys. **48**, 2171 (1972).

[80] V.J. Emery, Phys. Rev. B **14**, 2989 (1976).

[81] J.D. Cloizeaux and M. Gaudin, J. Math. Phys. **7**, 1384 (1966).

[82] D.S. Fisher and P.C. Hohenberg, Phys. Rev. B **37**, 4936 (1988).

[83] T. Matsubara and H. Matsuda, Prog. Theor. Phys. **16**, 569 (1956); **17**, 19 (1957).

[84] K. Kubo and T. Kishi, Phys. Rev. Lett. **61**, 2585 (1988).

[85] For example, J.D. Reger and A.P. Young, Phys. Rev. B **37**, 5978 (1988); R.R.P. Singh, Phys. Rev. B **39**, 9760 (1989); S. Liang, Phys. Rev. B **42**, 6555 (1990). For a detailed review, see E. Manousakis, Rev. Mod. Phys. **63**, 1 (1991).

[86] J. Goldstone, Nuovo Cimento **19**, 154 (1961); J. Goldstone, A. Salam and S. Weinberg, Phys. Rev. **127**, 965 (1962).

[87] H.G. Evertz, G. Lana and M. Marcu, Phys. Rev. Lett. **70**, 875 (1993); N. Kawashima and J.E. Gubernatis, Phys. Rev. E **51**, 1547 (1995).

[88] C.J. Hamer, Z. Weihong and P. Arndt, Phys. Rev. B **46**, 6276 (1992).

[89] Z. Weihong, J. Oitmaa and C.J. Hamer, Phys. Rev. B **43**, 8321 (1991).

[90] L. Néel, Ann. de Phys. **5**, 232 (1936).

[91] K. Yosida, Prog. Theor. Phys. **6**, 691 (1951).

[92] M.-C. Cha, M.P.A. Fisher, S.M. Girvin, M. Wallin and A.P. Young, Phys. Rev. B **44**, 6883 (1991).

[93] C. Bruder, R. Fazio, A. Kampf, A. van Otterlo and G. Schön, Phys. Scr. **42**, 159 (1992); C. Bruder, R. Fazio and G. Schön, Phys. Rev. B **47**, 342 (1993).

[94] A. van Otterlo and K.-H. Wagenblast, Phys. Rev. Lett. **72**, 3598 (1994); A. van Otterlo, Phys. Rev. B **52**, 16176 (1995).

[95] R.T. Scalettar, G.G. Batrouni, A.P. Kampf and G.T. Zimanyi, Phys. Rev. B **51**, 8467 (1995); G.G. Batrouni, R.T. Scalettar, G.T. Zimanyi and A.P. Kampf, Phys. Rev. Lett. **74**, 2527 (1995).

24

現代思想の源流と未来の志向性の哲学